J Neurophysiol 107: 1979–1995, 2012.
First published December 14, 2011; doi:10.1152/jn.00625.2011.

A system for recording neural activity chronically and simultaneously from multiple cortical and subcortical regions in nonhuman primates

Joseph Feingold,[1,2]* Theresa M. Desrochers,[1,3]* Naotaka Fujii,[4]* Ray Harlan,[5] Patrick L. Tierney,[1,3] Hideki Shimazu,[1,3] Ken-ichi Amemori,[1,3] and Ann M. Graybiel[1,3]

[1]*McGovern Institute for Brain Research,* [2]*Harvard-MIT Division of Health, Sciences and Technology, and* [3]*Brain and Cognitive Sciences, Massachusetts Institute of Technology, Cambridge, Massachusetts;* [4]*Brain Science Institute, RIKEN, Saitama, Japan;* [5]*Specialty Machining, Wayland, Massachusetts*

Submitted 2 July 2011; accepted in final form 13 December 2011

Feingold J, Desrochers TM, Fujii N, Harlan R, Tierney PL, Shimazu H, Amemori K, Graybiel AM. A system for recording neural activity chronically and simultaneously from multiple cortical and subcortical regions in nonhuman primates. *J Neurophysiol* 107: 1979–1995, 2012. First published December 14, 2011; doi:10.1152/jn.00625.2011.—A major goal of neuroscience is to understand the functions of networks of neurons in cognition and behavior. Recent work has focused on implanting arrays of ~100 immovable electrodes or smaller numbers of individually adjustable electrodes, designed to target a few cortical areas. We have developed a recording system that allows the independent movement of hundreds of electrodes chronically implanted in several cortical and subcortical structures. We have tested this system in macaque monkeys, recording simultaneously from up to 127 electrodes in 14 brain regions for up to one year at a time. A key advantage of the system is that it can be used to sample different combinations of sites over prolonged periods, generating multiple snapshots of network activity from a single implant. Used in conjunction with microstimulation and injection methods, this versatile system represents a powerful tool for studying neural network activity in the primate brain.

electrophysiology; microstimulation; injection; cellular network

MICROELECTRODE-BASED RECORDING techniques provide the most direct measure of electrical activity in the brains of behaving animals. Extracellular recordings of neural signals in the awake, behaving monkey, pioneered by Evarts (1968), have shaped our understanding of how the primate brain operates as animals perceive the world, make decisions, and select appropriate actions to reach goals. Despite their remarkable contributions to neuroscience, these classic single-electrode recording methods fall short of the capability of measuring the activity of many neurons simultaneously. Solving this problem is critical, given the widely recognized need to analyze neural computations across distributed networks (Alexander et al. 1986; Cohen and Maunsell 2009; Pesaran et al. 2008), including both cortical and subcortical nodes, the interactions among which are crucial to the function of the entire network (Contreras et al. 1996; Pennartz et al. 2009; Siapas et al. 2005; Sommer and Wurtz 2008) and to the pathophysiology of major neurological diseases (Graybiel and Rauch 2000; Hammond et al. 2007; Rivlin-Etzion et al. 2006).

To increase the number of simultaneously recorded sites in the monkey brain, three approaches have been pursued. First, neuronal activity has been recorded simultaneously from multiple brain structures (Hernandez et al. 2008; Pasupathy and Miller 2005) or from multiple sites within a single structure (Baker et al. 1999; Courtemanche et al. 2003; Gray et al. 2007) in acute preparations. Second, chronically implanted arrays of immovable electrodes have increased rates of data acquisition by at least one order of magnitude over acute single-electrode techniques (Nicolelis et al. 2003; Nordhausen et al. 1996; Suner et al. 2005; Vetter et al. 2004; Ward et al. 2009). The pioneering use of these arrays has led to new insights into the correlated activity of multiple neurons (Cohen and Maunsell 2009), as well as to novel therapies centered on brain-machine interfaces for human patients (Carmena et al. 2003; Hochberg et al. 2006; Velliste et al. 2008). Third, small numbers of chronically implanted adjustable-depth electrodes have been used to afford some control over the placement of electrodes postimplantation (Jackson and Fetz 2007; Sun et al. 2006; Swadlow et al. 2005). Other techniques (deCharms et al. 1999; Ecker et al. 2010; Lei et al. 2004), including those adapted from methods used in rodents (Jog et al. 2002; Johnson and Welsh 2003; Yamamoto and Wilson 2008), have begun to be scaled up to record simultaneously from more than one structure in the monkey.

There remains, however, a key need to permit the independent movement of large numbers of electrodes implanted for prolonged periods of time in multiple brain structures. To address this need, we developed a system for recording simultaneously from hundreds of independently movable electrodes implanted in cortical and subcortical sites in the monkey. The main technological advances we made include designing novel screw-based microdrives to maximize the density of independently movable electrodes, pioneering the use of large craniotomies and appropriate chambers to maximize the number of targeted brain structures, and developing the detailed procedures required to optimize recordings from chronically implanted electrodes. Using this Chronic Independently Movable Electrode (ChIME) system, we recorded from up to 127 electrodes simultaneously in 14 brain regions with implants lasting up to a year. Like chronically implanted arrays, the ChIME system allows repeated sampling of the same sites from session to session, and, like acute methods, it enables the sampling of multiple sites along individual recording tracks, providing an opportunity to improve the unit isolation at each site by adjusting the depth of the electrode. The implant procedure is reversible, and individual monkeys can receive multiple implants in succession, with different configurations

* J Feingold, T. Desrochers, and N. Fujii contributed equally

Address for reprint requests and other correspondence: A. M. Graybiel, Massachusetts Institute of Technology, 43 Vassar St., Bldg. 46-6133, Cambridge, MA 02139 (e-mail: graybiel@mit.edu).

of microdrives, targeting the same or different brain regions. The ChIME system is straightforward to use and highly flexible; the number and locations of the microdrives can be completely reconfigured from implant to implant, and the microdrives can be used with many different types of electrodes and in combination with electrical stimulation, pharmacological injection, and optogenetic techniques. These are essential tools for determining the function of interconnected networks in the brain. The ChIME system thus represents a novel synthesis of numerous critical capabilities into a single, integrated platform suitable for studying the electrophysiology of the nonhuman primate brain, the definitive animal model for the human brain.

MATERIALS AND METHODS

To obtain neural recordings from chronically implanted electrodes, two implantation phases were required. In the first phase, the recording chamber was permanently secured to the monkey's skull and craniotomies were performed (see *Surgical procedures*). In the second phase, the electrodes were implanted using a grid and microdrives that could be removed, repositioned, and reused in the same animal (see *Chronic implant procedure*). Here we describe in detail all of the procedures needed to obtain neural recordings, in the order in which they were performed.

Surgical procedures. Procedures were performed under sterile conditions on anesthetized monkeys placed in a standard stereotaxic apparatus, in accordance with National Institutes of Health guidelines and as approved by the Massachusetts Institute of Technology's Committee on Animal Care. Before the chamber implant procedure, in a separate procedure, a mold of the skull was made (VP Mix; Henry Schein, Melville, NY) and subsequently used to create a plastic chamber (Delrin, DuPont, DE; Specialty Machining, Wayland, MA). The curved bottom surface of the chamber was machined to fit the contours of the skull precisely. On the basis of preoperative MRIs of the monkey (T1 and T2 weighted structural images, 1.5–3.0 Tesla; Siemens, Munich, Germany) and in accordance with Rhesus monkey atlases, the chamber was positioned under stereotaxic guidance to facilitate recordings from target brain areas. The chamber was placed over a single hemisphere or over both hemispheres, spanning the midline. To minimize the risks of hemorrhage, damage to the dura mater, and brain swelling that might result from performing a large craniotomy in a single procedure, we performed multiple craniotomies in separate procedures, gradually enlarging the opening in the skull up to 40 mm $\times$ 40 mm. We also avoided the use of isoflurane as an anesthetic, which can induce edema and increased intracranial pressure (Santra and Das 2009).

During the initial procedure, one or two bone flaps, 10 mm $\times$ 20 mm, were turned over the intended recording regions. Opening these windows in the bone allowed us to access selected brain regions (e.g., the frontal eye fields) for electrophysiological mapping, without having to perform the riskier large-scale craniotomy in a single procedure. The chamber was then secured to the skull with radioopaque bone cement (Palacos, Zimmer, OH), anchored by ceramic screws (Thomas Recording, Geissen, Germany) in the skull. Divots on the outside of the lower part of the chamber facilitated the adhesion of the bone cement. The chamber was designed so that the bottom of the removable grid into which the microdrives can be inserted would be ~10 mm above the highest point on the skull, leaving room for fluid to escape through the side ports, rather than rise above the grid. The placement of the chamber was confirmed postoperatively with a structural MRI. As a precaution against swelling, craniotomies were treated with a dilute solution of a steroidal anti-inflammatory (dexamethasone), applied directly within the chamber during the postoperative recovery period.

At least 1 mo after the chamber implant, the remaining bone covered by the chamber was removed in one or more procedures, depending on the animal and the experimental schedule. Ultimately, sufficient bone was removed to allow access to the entire volume of brain beneath the chamber, resulting in a single opening in the skull of up to 1600 mm^2. Following recovery, additional physiological mapping was performed to reconfirm the 3D coordinates of the brain in relation to the grid. Additional minor surgical procedures were performed periodically to remove growing bone and to thin the dura mater and overlying granulation tissue.

Electrophysiological mapping. Initially, under the guidance of structural MRIs, the cortex and striatum of each monkey was mapped to determine the locations relative to the grid of known brain landmarks. In each mapping session, a 7-mm-thick rectangular plastic grid (area: 30 $\times$ 30 mm^2, 30 $\times$ 40 mm^2, 30 $\times$ 50 mm^2 or 40 $\times$ 40 mm^2; Specialty Machining; Fig. 1*C*) was inserted into the recording chamber and secured in place with a screw in each corner. Depending on the size of the grid, its holes (0.025 mm in diameter, spaced 1 mm center to center) could provide access to the brain across an area of up to 1600 mm^2. The holes in some grids were offset such that a 90° rotation would provide access to tracks that are shifted by 0.5 mm from those accessible in the original orientation. This design enabled sampling from nonoverlapping recording tracks when accessing the underlying brain through the same grid holes in successive chronic implants.

In each mapping session, up to 12 epoxy-insulated tungsten microelectrodes (1–2 MOhm at 1 kHz, 110–130 mm long, 125-μm shank, ~3-μm diameter tip; Frederick Haer, Bowdoin, ME) glued to screw microdrives (Fig. 1*B*) were acutely implanted in the brain, using sharp stainless steel guide tubes to penetrate the dura mater while protecting the tips of the electrodes. Neuronal responses were characterized by standard somatosensory, visual, and auditory tests and by manipulation of the limbs and electrical microstimulation (trains of 24–64 250-μs wide biphasic pulses, 333 Hz, 10–150 μA; Master-8; A.M.P.I., Jerusalem, Israel, and Bak Electronics, Mount Airy, MD). Several sessions were performed to map the somatotopic organization of the motor and oculomotor cortical areas, including primary motor cortex (M1; Strick and Preston 1982), frontal eye fields (FEF, Funahashi et al. 1989; Sommer and Wurtz 2000), supplementary motor area and presupplementary motor area (SMA and pSMA, Luppino et al. 1991; Matsuzaka et al. 1992; Mitz and Wise 1987), and to confirm the depths of the caudate nucleus (CN), putamen (Put), and other subcortical targets, as needed. The dorsolateral prefrontal cortex (dlPFC) was defined as the area rostral to the FEF, surrounding the principal sulcus and corresponding to Brodmann Area 9/46.

Chronic implant preparation. Depending on the experiment and based on the MRIs and the results of electrophysiological mapping, the desired number and locations of electrodes were determined. Care was taken to avoid implanting electrodes too close to the midline, to prevent damage to the central sinus. The electrodes were loaded onto custom-made screw-based microdrives (Specialty Machining). Each microdrive consisted of one to three groups of three adjacent screws each (length, 0.825 in; 160 threads per inch, so that six 360° turns = 0.9525 mm of vertical travel distance), spaced 1 mm apart, and supported by a plastic frame. A pair of stainless steel pins on the bottom of the microdrive frame fit into grid holes and was used to secure the microdrive to the grid inside the chamber rigidly. Unlike conventional screw-based microdrive designs (Nichols et al. 1998), no additional pins were used above the surface of the grid to fix each microdrive in place. This novel design reduced the size of the footprint of the microdrive on the grid, thereby increasing the density of the recording tracks. The microdrive was designed so that the heads of the screws were flush with the top of the microdrive and could be turned with a flat-head screwdriver (Fig. 1, *A*, *B*, and *E*). Each screw was threaded through a 5-mm-long plastic sled with a slot to which one or more electrodes could be glued. The screws rested on the bottom of the microdrive frame, so that turning a screw would cause

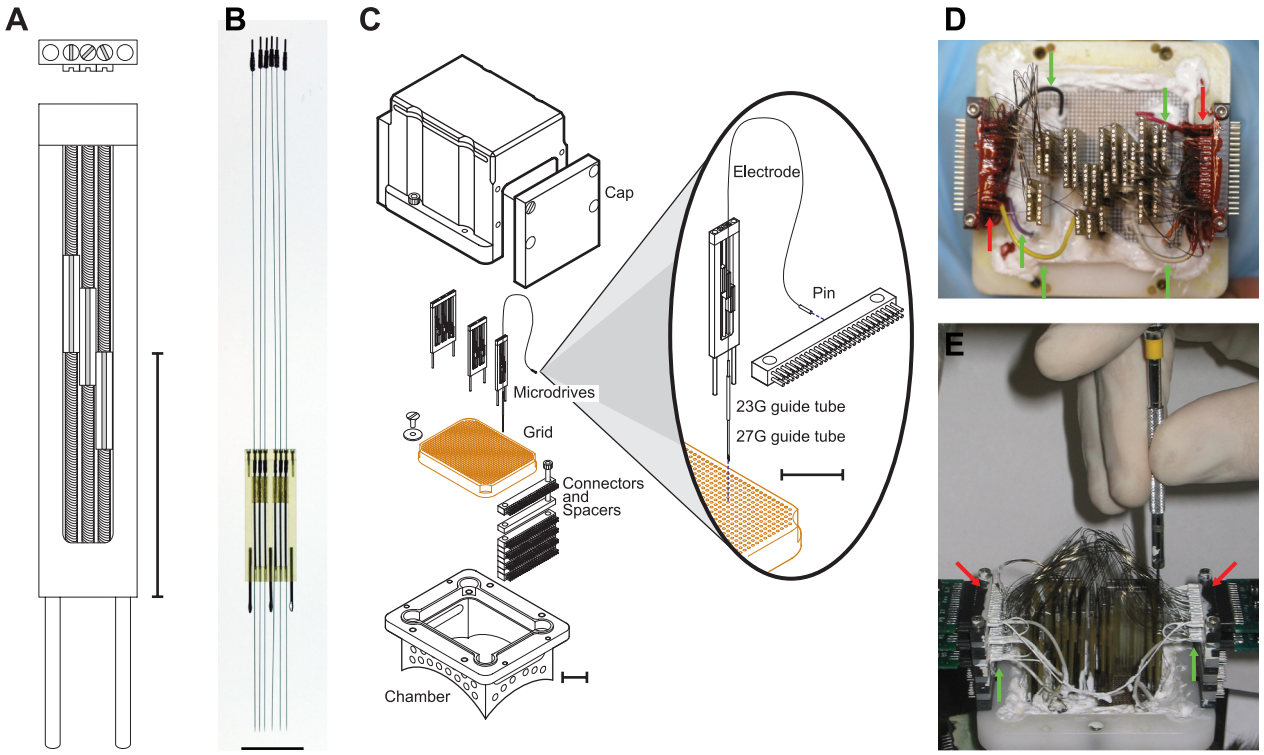

Fig. 1. Reconfigurable chronic electrode implant system. All scale bars = 1 cm. *A*: computer-aided design (CAD) drawings of top and front views of a nonloaded 3-screw microdrive. Electrodes can be glued to the slotted plastic sled attached to each screw. When the screw is turned, the plastic sled moves along the screw shaft, guiding the attached electrode through a grid hole immediately adjacent to the row of grid holes covered by the drive itself, thereby maximizing the number of grid holes that can be targeted simultaneously in a single implant. *B*: 6-screw microdrive with a conventional tungsten microelectrode glued to the plastic sled on each screw. There is a connecting pin attached to the top of each electrode (see MATERIALS AND METHODS). Note that the plastic of which the manipulator is made is translucent, allowing one to see the 2 screws imbedded in the top section of the manipulator to secure it to the body of the manipulator in the upper corners and the tops of the 3 pins embedded in the bottom of the manipulator that are used to secure the manipulator to the grid. *C*: exploded-view CAD drawing of chamber cap, microdrives (left to right, 9, 6, or 3 screws for driving electrodes), grid, connector strips, and chamber. Side ports in the chamber below the level of the grid provide access for cleaning and observation of the granulation tissue over the dura mater. A ridge along the top of the chamber prevents fluid from contaminating the microdrives and connector strips. The chamber cap has upper slots for ventilation and removable side panels for easy access to the connector strips. *Inset*: schematic of a 3-screw microdrive loaded with a single electrode. A beveled 27-gauge guide tube is used for punching through the dura mater and fits inside a shorter 23-gauge tube to minimize friction with the grid hole. *D*: top view of 117 electrodes in monkey H (implant 1). Insulating varnish used to isolate connecting pins is red (red arrows). Black, red, yellow, purple, and gray wires are the leads from tubes used for reference (green arrows). The silicon used to seal the grid holes and around the edges of the top of the grid is white. *E*: anterior view of an implant of 111 electrodes in monkey J. On the sides, 5 green preamplifiers are connected to the electrode leads via black connector strips (red arrows). White silicone covers the surface of the grid at the base of the microdrives to promote dryness above the grid. Reference wires, ground wires, and the exposed surfaces of pins are insulated with paint (green arrows indicate pin row locations). The depth of each electrode can be manipulated independently by turning the appropriate microdrive screw with a small flat-head screwdriver as shown.

the attached sled to move along the shaft of the screw. The sleds were arranged in groups of three such that the side of each sled was directly abutting either the plastic frame of the microdrive or another sled (Fig. 1*A*). This arrangement prevented the sled from spinning around the screw rather than traveling up and down along the shaft when the screw was turned. Because the sleds on adjacent screws were controlled independently, it was possible to raise or lower an individual sled such that it would no longer be in contact with its neighbor. As this would preclude the possibility of making further adjustments to the depths of the attached electrodes, the relative positions of the sleds had to be monitored so that each sled maintained at least ~0.5 mm of overlap with its neighbors. The sleds guided the electrodes through the grid holes in a row immediately adjacent to the grid holes occupied by the microdrive itself. Each microdrive targeting three, six, or nine recording tracks occupied a total of 9, 16, or 23 grid holes, respectively, including the grid holes used for the electrodes.

Before the implant procedure, the grid was prepared in the following manner. First, the entire top and under side of the grid was covered in a general-purpose silicone sealant to prevent fluid from below the grid from contaminating the space above the grid. After curing, the silicone was cleared with a 23-gauge needle from the grid holes needed for the implant. Bare copper wire for carrying the ground was looped below the grid, and the free ends were fed through cleared grid holes and capped with pins to interface with the connectors. In some implants, the copper wire was soldered to a piece of flattened copper mesh, designed to rest over as large a portion of the granulation tissue as possible (without obstructing the path of the electrodes). The outer guide tubes (23-gauge, extra thin wall) of a pair of telescoping guide tubes (designed to protect each electrode) were then inserted into the holes cleared for electrode tracks. The length of each tube was prepared such that, if one end were flush with the top of the grid, the other end would not touch the surface of the granulation tissue above the dura mater. Because of the friction between the 23-gauge guide tubes and the grid holes with silicone residue, these guide tubes could not slip out of the holes. Distances from the top of the grid to the top of the tissue ranged from 22–30 mm, depending on the implant and location within the chamber. Implanted electrodes that did not record unit activity or 23-gauge stainless steel tubes resting on top of the tissue were used for reference. The tubes were connected to the preamplifiers via a small, insulated wire soldered to the top of the tube (above the surface of the grid; e.g., Fig. 1*D*, black, purple, yellow, red, and gray wires near the corners of the grid indicated by green arrows).

The entire grid construct was bathed in 70% ethyl alcohol before the implant procedure for disinfecting.

The microdrives and electrodes were prepared in parallel with the grid. First, connector pins were crimped onto the ends of the electrodes [same as mapping electrodes or Parylene-coated tungsten or platinum/iridium (Pt/Ir), 125-μm shank diameter, impedance < 1.5 MΩ; We Sense, Israel] and then glued (2-h epoxy, extra slow cure). Second, the impedance of each electrode was tested to confirm that it fell within an acceptable range (0.5–1.5 MOhms). Third, each electrode was glued to a slotted sled on one microdrive screw so that, upon implanting, the recording tip of the electrode would be at a desired depth below the grid. After the glue cured, securing the electrodes to the microdrive, a sharp-edged stainless steel guide tube (27-gauge, regular wall hypodermic disposable needle or custom-cut, beveled tubing) was slipped over the shank of each electrode and left covering the tip to protect it during the implant procedure. These 27-gauge guide tubes were cut to be a length that would span the predetermined distance from the top of the grid to the top of the brain and allow for some extra length to manipulate them during the implant procedure (typically 30–40 mm total length). The guide tubes were filled with mineral oil to keep out blood and other fluids. The electrode leads of each loaded microdrive were grouped using labeled, folded paper slips, preventing the leads from tangling with those from the other microdrives during the implant procedure.

Chronic implant procedure. The implant procedure was performed under aseptic conditions, with the monkey under general anesthesia (ketamine, xylazine, and atropine) and the head fixed within a stereotaxic apparatus. After thoroughly cleaning and drying the chamber and the grid, we applied silicone sealant around the outer edge of the grid. The grid was inserted into the chamber and secured to it with four screws and washers in the corners. Then, working from the center of the implant outward, each microdrive was implanted in turn, as follows. First, the microdrive was carefully positioned above the target grid holes. The experimenter's (nondominant) hand held the main section of the microdrive to ensure that the 27-gauge guide tubes covering the electrodes did not slip off, while the other (dominant) hand used forceps to lower the tips of those guide tubes into the 23-gauge guide tubes that had been inserted into the grid before the implant procedure (during the preparation phase). Once all the sharp guide tubes for a given microdrive were properly situated with the ends inserted into the corresponding 23-gauge guide tubes, the microdrive was held perpendicular to the grid and the microdrives with electrodes attached and the 27-gauge guide tubes were slowly lowered in tandem. The tips of the 27-gauge guide tubes were just touching the surface of the tissue covering the brain (lowering was stopped once resistance was felt), and the electrode tips were still protected within the guide tubes. One by one, the 27-gauge tubes were then used to punch small holes through the dura mater by applying careful downward pressure using forceps or fine needle holders. Once holes in the dura mater over all the intended tracks for a given microdrive had been punched, the microdrive was lowered slightly further to test the smooth passage of the electrodes through the guide tubes and into the brain. If this succeeded, then the 27-gauge guide tubes were lifted somewhat so they would not remain in the brain but maintain contact with the overlying tissue. The microdrive was then slowly lowered into its final position with its bottom pins fitting into the grid holes, until the bottom of the microdrive frame became flush with the surface of the grid. Any fluid that came up through the guide tubes to the top of the grid as a result of the implantation process was removed using cotton swabs. During the electrode implantation, openings in the sides of the chamber were used to monitor visually the tissue beneath the grid for excessive compression, bleeding, or other complications, as well as to remove any excess fluid, to minimize the possibility of fluid traveling up the guide tubes.

After implantation of all the electrodes, a bead of silicone sealant was applied along the upper junction of the chamber and grid and the grid anchor screws were also covered with silicone. Any cleared holes in the grid not filled by implant components were also filled in. The pins from the ends of the electrode leads, references, and ground wires were then plugged into the appropriate spots along the connector strips. Efforts were made to minimize crisscrossing of the leads above the microdrives. Finally, all the wires were carefully bent with forceps to accommodate the connectors fastened to the edges of the chamber, and a thick coat of varnish was applied to protect and insulate them (completed implant, Fig. 1*D*). Plastic spacers (Fig. 1, *C–E*) were used in between the connectors to adjust their heights as needed to accommodate the preamplifiers. The location of holes used to screw the connectors to the chamber and the dimensions of the plastic spacers could easily be adjusted to accommodate different sizes or configurations of preamplifiers. Postimplant monitoring for infection and other complications was performed as part of the daily recording sessions and maintenance (see next section).

Recording sessions and implant maintenance. During the first few weeks of a chronic implant, electrodes were slowly lowered to their initial recording positions in the brain, the earliest points at which unit activity could be detected in the target structures. Once a sufficiently large fraction of electrodes had reached their targets, recordings commenced in daily sessions. Either at the start of recording sessions or in between them (on nonrecording days), a subset of electrodes was advanced carefully in ~20-μm steps, to improve the quality of units or to isolate new ones. On any given day, no more than 1/3 of the total electrodes in the implant were moved, and an effort was made not to move adjacent electrodes, to promote the stability of recorded signals.

Large slots in the lower portion of the chamber (Fig. 1*C*) provided access to the underside of the grid for daily cleaning and observation of the surface of the granulation tissue, which grew with time to cover the dura mater. This granulation tissue effectively sealed the brain from the underside of the grid and chamber. At the start of each session, the chamber beneath the grid was flushed thoroughly with sterile saline via these side ports. Depending on the monkey and the chronic implant, this was followed by diluted (20:1) Novalsan Solution (chlorhexidine diacetate 2%) or Betadine Solution (povidone-iodine 10%) 2–5 times per week. Possible infections, as indicated by the type and amount of discharge, were treated with diluted antibiotic applied inside the chamber. Systemic administration of antibiotics was rarely used. Topical antibiotic ointment was occasionally applied along the margins of the chamber. With these precautions, the chambers could be maintained for up to five years (Chamber lifetime, Table 1).

The chamber beneath the grid was filled with saline for the duration of the recording session. Before some sessions, the saline was mixed with viscous methyl cellulose to reduce noise resulting from the motion of the saline. When necessary, application of petroleum jelly or silicon grease to the electrode leads between the tops of the microdrives and the connectors effectively dampened mechanical vibrations of the electrodes. Additionally, silicon grease was occasionally used to fill the space between the electrodes and guide tubes, sealing the tops of the tubes, while permitting the free movement of the electrodes.

Over the course of the implant, the space above the grid was kept as dry and clean as possible to preserve the quality of recorded signals and the ability to manipulate the depths of electrodes with the microdrives. In addition to sealing the grid with silicone during the implant procedure (see above), the side slots in the chamber beneath the grid could be left partially open, indefinitely, to prevent potential fluid buildup. Further protection from fluid above the grid was provided by a raised ridge around the top of the inner surface of the chamber (surrounding the grid) that served as a dam.

In between experimental sessions, the chamber was covered with either a raised cap, while electrodes were implanted in the brain, or a flat cap, otherwise (Fig. 1*C*, *top*). The side panels on the raised cap could be removed to connect preamplifiers to the connector strips without having to remove the main portion of the cap, protecting the

Table 1. *Summary of implant statistics*

Monkey ID	G	Y	H	J	K	L	M	Overall
Chamber lifetime, yr	3.2	4.6	3.0	3.7	2.2	2.5	4.5	3.4
Implant duration, days	189.5	265	121	264	36.3	53	40.5	130.9
Brain areas targeted	7	6	14	10	4	4	6	7.3
Implanted electrodes	84	87	119	115	38.7	39	36	74.8
Recording sessions	75	101.5	24	28	18	20.5	17.5	38.1
Unit-recording electrodes, total	2196	1816.5	696	723	411	359	253	875.9
Yield:								
1st day of recording	50%	30%	35%	22%	30%	17%	24%	30%
Maximum	60%	36%	39%	32%	79%	78%	71%	57%
Minimum	24%	8%	10%	12%	21%	8%	24%	15%
Mean across all recording sessions ± SD	35 ± 10%	21 ± 6%	25 ± 7%	23 ± 7%	56 ± 17%	47 ± 21%	43 ± 18%	31 ± 16%
Mean unit-recording electrodes per session	29	19	29	25	21	19	18	23
Unit-recording electrodes with activity on at least 1 day	83%	81%	82%	67%	77%	73%	71%	77%

Values for each monkey were averaged across implants. Overall values were calculated from grand averages across all monkeys and implants.

electrode leads. Ventilation slots along the nonremovable ends of the raised cap helped to keep the space above the grid cool and dry.

Neuronal signals were amplified and filtered [600–6,000 Hz for spikes, and 1–475 Hz for local field potentials (LFPs)] by the Cheetah system (Neuralynx, Bozeman, MT). Spike waveforms (32-kHz sampling rate) and LFP signals (2 kHz) were continuously collected during daily recording sessions. The Cheetah system was configured to accommodate up to 128 single electrodes along with eight analog input channels (for behavioral data). At the start of each recording session, custom software was used to configure each electrode channel to record either spike or LFP data. Spike and LFP signals could be recorded simultaneously from up to 32 electrodes. Each neural (spike or LFP) data channel was stored to a separate file for offline analysis.

In some implants, the impedance of the electrodes was measured periodically, and those with high impedance (>2 MOhm) were stimulated (100–200-ms trains of biphasic pulses at 1 kHz, <20 μA, Master-8; A.M.P.I. and Bak Electronics). Stimulation was repeated up to five times or until the impedance fell below 2 MOhm. Poststimulation impedance values were measured and recorded.

Electrical stimulation experiments. Stimulation experiments were conducted with a chronic implant of 48 independently movable electrodes targeting the anterior cingulate cortex (ACC), cingulate motor area (CMA), CN, and dlPFC. In each trial a single bipolar, biphasic pulse (current amplitude: 200 μA, cathodal-anodal pulse duration: 400 μs) was delivered between two of the Pt/Ir electrodes chronically implanted in the ACC (4 mm apart). The responses of single units in the ACC and CMA were analyzed by binning the spike counts of each unit in a 20-ms window surrounding the stimulus delivery. The analysis was repeated for two bin sizes (0.1 ms and 1 ms). Bins with spike counts beyond the 99% confidence limits were defined as statistically significant. Those units exhibiting significant responses irrespective of bin size were considered to be modulated significantly by the electrical stimulation.

Stimulation experiments in the dlPFC were performed with a chronic implant of 24 independently movable tungsten electrodes (12 each in dlPFC and CN). Four of the dlPFC electrodes (2 each in areas 9L and 46) were used for delivering electrical stimuli. In each of 40 trials, spaced 5 s apart, a single monopolar, biphasic pulse (current amplitude: 20 μA, cathodal-anodal pulse duration: 300 μs) was delivered. LFPs were recorded from eight electrodes in the CN (2 mm apart in a 4 × 4 configuration). LFPs were low-pass filtered at 20 Hz, and stimulation-triggered waveform averages were computed on 400 ms of LFP data centered on the onset of stimulation. Significant modulation of waveform averages was detected by comparing the poststimulation activity to the 95% confidence limits estimated from the prestimulation activity.

Pharmacological microinjection experiments. A microelectrode nested within a steel cannula was used to record electrophysiological activity during local drug infusion. The cannula was connected via polyethylene tubing to a tabletop pump (Harvard Apparatus, Cambridge, MA). Drugs were delivered at a rate of 100 nl/min for 2 min. Periods of significant changes in firing rate were detected using a sliding bin average, as follows. Spike counts were aggregated into 10-s bins, and the bin values underwent three-point smoothing. Baseline activity was defined as the mean spike count over the 5 min immediately preceding drug infusion. The onset of a significant change in firing rate was defined as the first of 10 consecutive bins with values at least 2 SD from the baseline. Response offset was defined as the first of 10 consecutive bins with values within 2 SD of the baseline.

Implant removal. At the end of a chronic implant, the electrodes were slowly raised to their initial depths, over a few daily sessions. With the alert monkey head-fixed, the implant was then removed in a single procedure. First, the electrode leads above the microdrives and reference and ground wires were cut, and the connector strips were unscrewed from the chamber. Each microdrive was then removed by first ensuring that the electrodes had been retracted as far as possible, using forceps to raise guide tubes and then gently using force perpendicular to the grid, to extract the manipulator. Once all the manipulators had been removed in this manner, the silicone sealing the grid was stripped away and the grid was removed by unscrewing the corner screws. The chamber was then thoroughly rinsed with sterile saline. The monkey was allowed to recover for at least a few weeks before the next implant. The grid, microdrives, and most 23-gauge guide tubes that could be recovered for use in subsequent implants were cleaned with ethanol, bleach, acetone, and occasionally sonication. If needed, before the next implant, a small drop of oil was added to each of the plastic sleds that travel along the microdrive screws, to ensure free movement of the sled and minimal wear and tear on the plastic.

Histology. After experiments were completed, the monkey was perfused intracardially with fixative (0.9% NaCl followed by 4% paraformaldehyde in 0.1 M Na^{2+}/K^{-} PO_4 buffer, pH 7.4). Whenever possible, this was done before removing the final chronic implant. In some cases, electrolytic lesions (10 μA DC for 10 s, <15 sites) were made to mark locations in the brain relative to the grid. Conventional Nissl staining (60-μm-thick slices) was performed to visualize electrode tracks. The slices were analyzed to reconstruct the location of each electrode in each recording session. Tracks from earlier chronic implants were reconstructed on the assumption that the distance from the grid to the surface of the brain was constant across implants. In some monkeys, anatomical tracing software and 3D reconstruction (Neurolucida; MicroBrightField, Williston, VT) was used.

Data analysis. Single units were isolated, and individual waveforms were aligned on their peaks using an offline sorter (Plexon, Dallas, TX). As a measure of cluster quality, the signal-to-noise ratio (SNR) of sorted units was calculated as the amplitude of the mean waveform divided by twice the standard deviation of the noise (Suner

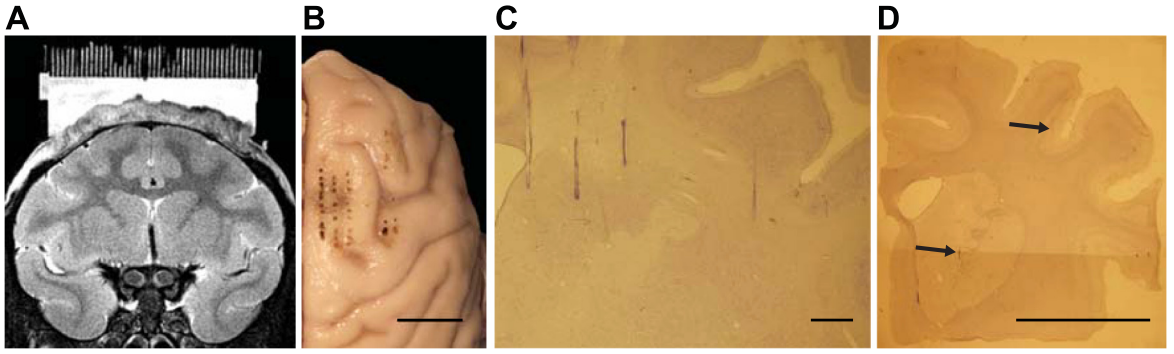

Fig. 2. Localization of electrodes simultaneously implanted in cortical and subcortical structures. *A*: coronal section from a T2-weighted structural MR image of monkey D showing the saline-filled grid and chamber above granulation tissue covering the intact dura mater. *B*: dorsal view of right hemisphere of monkey J's brain (anterior at top, medial wall at left). Scale bar = 1 cm. *C*: coronal cresyl violet-stained section from monkey H showing tracks of 3 electrodes targeting the caudate nucleus (CN) (*left*) and a fourth approaching the putamen (Put) (*right*), all from implant 3, which was removed after the monkey was perfused. Note the remarkably straight approach to the deep targets. Scale bar = 1 mm. *D*: coronal cresyl violet-stained section from monkey G showing tracks of electrodes that recorded from the CN (lower arrow) and dorsolateral prefrontal cortex (dlPFC) (upper arrow) in implant 2. Scale bar = 1 cm.

et al. 2005). Amplitude was defined as the maximum voltage minus the minimum voltage of the mean waveform. The standard deviation of the noise was calculated by subtracting the mean waveform from each individual waveform and taking the standard deviation across all the resulting values. Cluster stability was assessed using a measure of waveform similarity based on the linear correlation (r) values between average waveforms (Jackson and Fetz 2007). First, the mean and variance were taken for all samples in the unit waveform, regardless of time point. This mean was then subtracted from each waveform, and all resulting waveforms were normalized (divided) by the variance. The correlation was then calculated using the average resulting waveforms after mean subtraction and variance normalization. Cor-

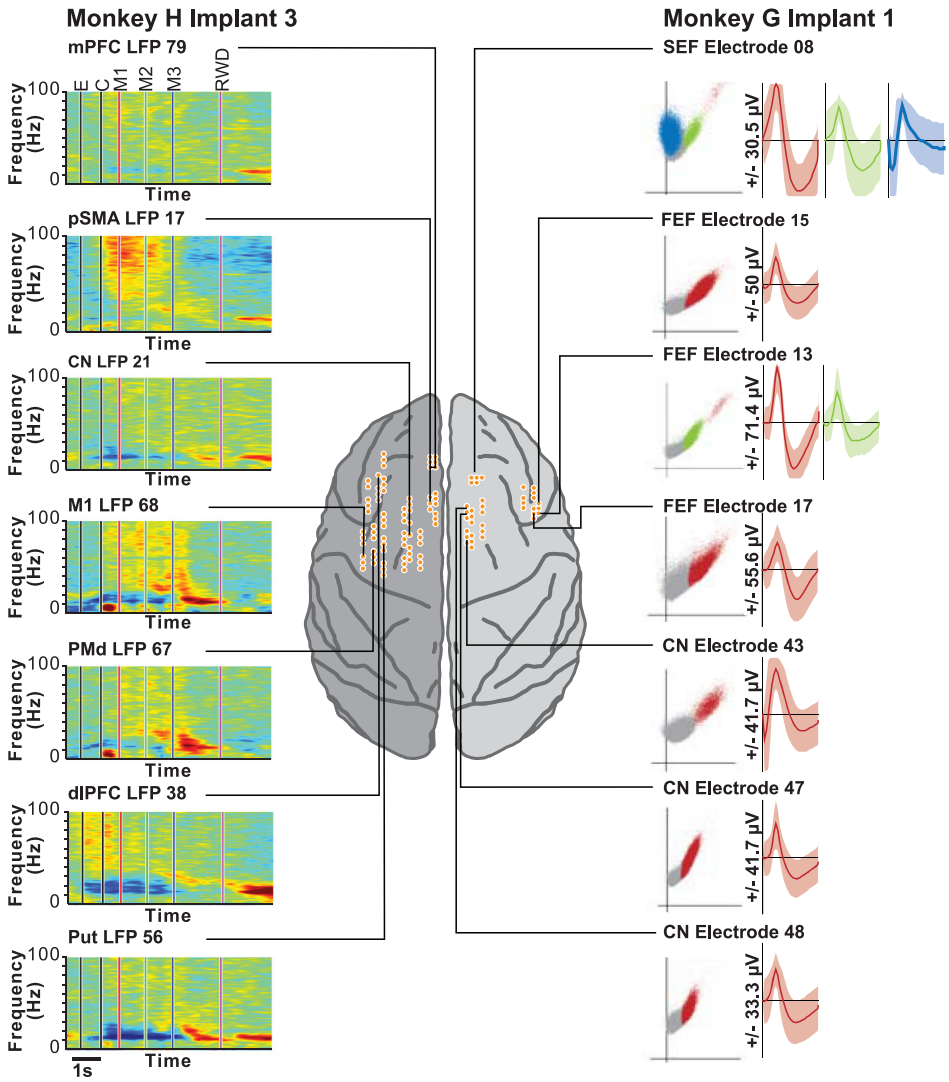

Fig. 3. Simultaneously recorded neural activity from multiple cortical and subcortical sites. *Center*: top-down view of macaque brain showing configuration of electrodes implanted in 1 hemisphere of each of 2 chronic implants (*left*, monkey H, implant 3; *right*, monkey G, implant 1; both monkeys were implanted bilaterally, but for purposes of visualization, only 1 hemisphere is shown for each monkey). Black lines identify the recording sites (projected onto the brain surface) for each sample neural signal shown. *Left*: spectrograms of local field potential (LFP) power simultaneously recorded from example sites on *day 159* of the implant, during performance of a joystick task, in which monkeys made three sequential joystick movements as instructed by visual cues. Spectrograms are aligned in windows on the following task events: trial start (E), cues onset (C), 1st-3rd joystick movement onset (M1–3) and reward delivery (RWD). The brain structure and electrode number are listed above each spectrogram. Power at each frequency indicated by color ranging from blue (−5 dB) to red (5 dB). *Right*: feature plots and average waveforms of units simultaneously recorded from the example sites on implant *day 126*, during performance of an oculomotor scan task, in which monkeys freely scanned visual targets to find the baited one. Feature plots show first principal component vs. peak-valley amplitude. Average waveforms are 1 ms in duration, and shading indicates ±3 SD. mPFC, medial prefrontal cortex; pSMA, presupplementary motor area; PMd, dorsal premotor cortex; SEF, supplementary eye fields; FEF, frontal eye fields.

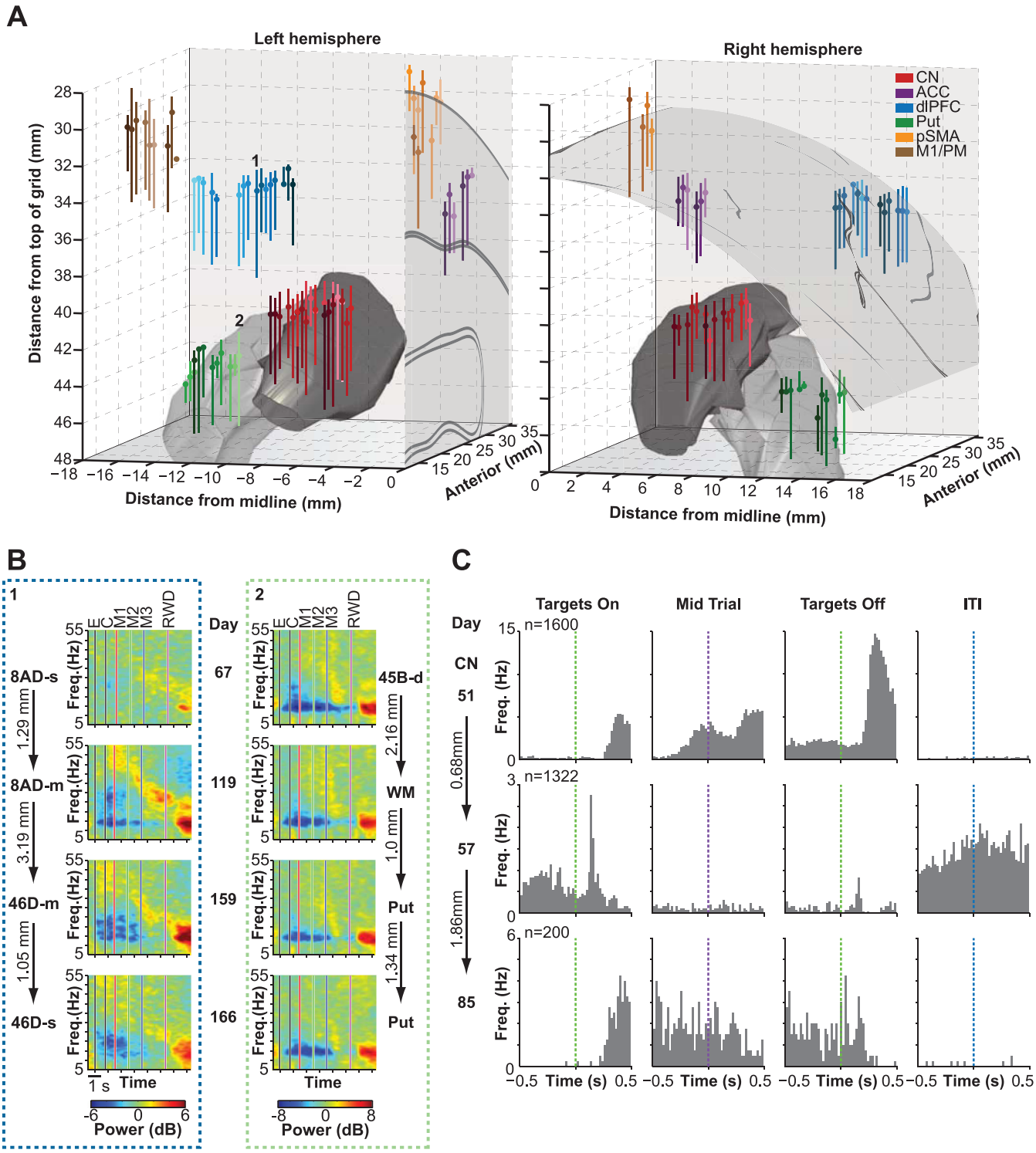

Fig. 4. Sampling at different depths across recording sessions. *A*: 3-dimensional schematic of all recording tracks for the duration of a single chronic bilateral implant (monkey H, implant 3, 172 days). Medial wall (*left*) and dorsal surface (*right*) of cortex shown in gray. Approximate locations of the CN (dark gray) and Put (light gray) are also indicated. Vertical colored lines represent the trajectories of the tips of the electrodes from the first through the last recording session of the implant. Dots indicate the electrode tip locations in a recording session midway through the course of the implant (*day 98*). Color of each line indicates targeted brain structure. *B*: spectrograms of LFP power recorded from 2 electrodes (labeled 1 and 2 in left hemisphere of *A*) in 4 sessions at 4 depths. Spectrograms follow same conventions as in Fig. 3. Day of implant, session-to-session change in depth and brain structure shown for each recording site (s, m, d indicate superficial, middle and deep layers of cortex, respectively). *C*: peri-event time histograms of single-unit spiking activity recorded in 3 sessions at 3 depths from an electrode targeting the CN in the right hemisphere (monkey G, implant 1, oculomotor scan task). Each row shows data from a single session and recording depth (implant day, number of trials, and change in depth shown). ACC, anterior cingulate cortex; PM, premotor cortex; WM, white matter; ITI, intertrial interval.

relation values between "different" units were obtained by correlating all units on each electrode with all units recorded on the other electrodes during the same recording session. Correlation values for "same" units were obtained by dividing each recording session into halves (by time) and then correlating the mean-subtracted, variance-normalized waveforms for the first half and second half for each electrode.

RESULTS

Reconfigurable chronic electrode implant system. We designed and implemented the ChIME system to obtain simultaneous recordings of neural activity from multiple, individually movable microelectrodes chronically implanted in cortical and subcortical structures of the primate brain. The key components of the ChIME system are compact screw-based microdrives that can be placed in nearly any configuration on a grid (Fig. 1). Improving upon the concept of the widely used (Pasupathy and Miller 2005) methods of Crist, Wurtz, and colleagues (Crist et al. 1988; Nichols et al. 1998) for acute, single-electrode recordings, the ChIME microdrives employ a novel mechanism that maximizes the density of independently movable electrodes. The grid can be inserted into a plastic chamber fixed to the skull to deliver electrodes to the underlying brain. Structural MRIs are used (Fig. 2*A*) to confirm the location of the grid holes relative to the target regions in the brain. We describe here the use of the system based on results from 16 implants of electrodes placed in cortical and subcortical sites in seven monkeys (Table 1). Preliminary experimental results based on the use of pilot versions of the ChIME system have been published elsewhere (Fujii and Graybiel 2005; Fujii et al. 2007).

Microdrives loaded with three, six, or nine individually movable electrodes were placed on a grid within the chamber, and the electrodes were lowered into the brain in a single implant procedure (see MATERIALS AND METHODS). Subsequently, across multiple daily sessions, the electrodes were advanced to their intended target sites. The depth of each electrode was controlled by turning the microdrive screw (158.75 μm/turn) to which it was attached. Implants were left in place for periods of weeks to months, during which the depths of individual electrodes were continually adjusted (maximum travel distance: 13 mm from initial implant depth). Following completion of the recordings, histological analysis was performed to reconstruct the locations of the electrodes (Fig. 2, *B–D*).

Simultaneously recorded neural activity from multiple cortical and subcortical sites. To test the ChIME system, we have used implants ranging in size from 27 to 127 electrodes and lasting from 22 to 365 days. In each implant, single-unit spike activity and LFPs were recorded simultaneously from electrodes implanted in 6–14 brain structures bilaterally, including medial prefrontal cortex (mPFC), dlPFC, FEF, supplementary eye fields (SEF), M1, premotor cortex (PM), SMA, pSMA, ACC, CMA, orbitofrontal cortex, parietal cortex, CN, Put, globus pallidus, thalamus, and amygdala. Recording sessions occurred on up to 59% of the days an implant was in place. In a single session, up to 57 electrodes recorded unit activity simultaneously along with 84 LFP signals. Under the constraints of the data-acquisition system that we used, when

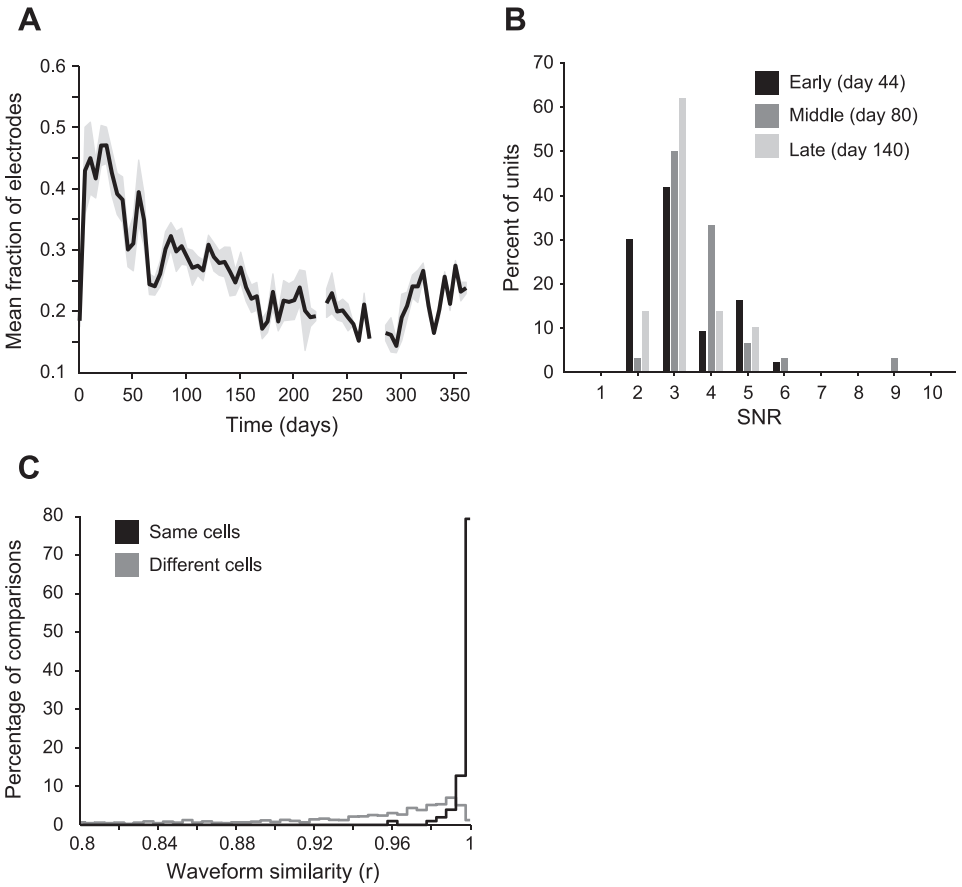

Fig. 5. Implant quality measures. *A*: mean yield over recording time across implants. The fraction of electrodes that recorded unit activity out of the total number of electrodes averaged over 16 implants in 7 monkeys. All electrodes were implanted in the brain on *day 0*. As not all implants have a yield measurement for each day of the implant (see Fig. 6), the mean yield (± SE) is shown for the pool of available data in 5-day bins. *B*: histogram of the signal-to-noise ratio (SNR) for all units recorded in 3 example sessions from monkey G, implant 1, which was in place for a total of 168 days. *C*: distribution of *r* values resulting from measuring the similarity of average waveforms pooled for 3 example sessions (*days 44*, *80*, and *140* as in *B*). Same unit similarity was measured between the average waveforms of the first half vs. the second half of the session it was recorded in. Different unit similarity was measured between all pairs of units recorded on different electrodes within the same session.

fewer units were recorded, up to 127 LFPs were recorded simultaneously.

We used the ChIME system to record neural signals simultaneously from several neocortical and subcortical regions participating in widely distributed brain networks. The left half of Fig. 3 gives examples of LFPs recorded simultaneously from the left hemisphere of a bilateral implant in monkey H, showing different activity patterns across seven regions, during performance of a joystick movement task. The right half of Fig. 3 shows examples of unit activity recorded simultaneously from the right hemisphere of a separate implant in monkey G, during performance of an oculomotor scan task. For each implant, all of the recording sites were accessed through a single craniotomy and grid.

Session-to-session adjustment of depths of individual electrodes. We have found that electrode depths can be adjusted either immediately before a recording session or on a previous day. Manipulating the depths of individual electrodes at different times enabled us to monitor activity from different combinations of sites within multiple regions across the recording sessions performed during a single implant (Fig. 4*A*). The vertical travel of the microdrives (up to 13 mm) enabled individual electrodes to progress through multiple brain structures over the course of a single chronic implant (Fig. 4*B*). Within a given brain structure, it was possible to record from sites at which neurons exhibited different activity profiles along a single track (Fig. 4*C*).

We defined the yield in each recording session as the fraction of electrodes that recorded single-unit activity (Liu et al. 2006; Muthuswamy et al. 2011; Ward et al. 2009). The average yield over all sessions was 31% (mean yield, Table 1), but the yield varied from implant to implant, ranging from 18 to 65%. The yield averaged across all implants decreased over months (Fig. 5*A*) although the time course of the yield differed across implants (Fig. 6). Implants with fewer electrodes and of shorter durations were associated with higher yields (Fig. 6, *right* vs. *left*; note difference in vertical scale). In most implants the yield converged within a few weeks to the overall mean value (31%). Our definition of the yield is conservative, capturing only the proportion of implanted electrodes that had single-unit activity on them, without attempting to differentiate multiple clusters recorded on the same electrode. To get a better sense of the numbers of resolvable single units recorded with the ChIME system, we also computed the yield in terms of the proportion of distinct single units per electrode for three implants in two monkeys (Fig. 6, *B*, *C*, and *I*, gray lines). The resulting yield in units matched or exceeded the results from the analysis based on our more conservative definition. We further analyzed the SNR of the waveforms of the single units recorded in three sessions. We found that all of the clusters had an SNR >2, which, using a previously published categoriza-

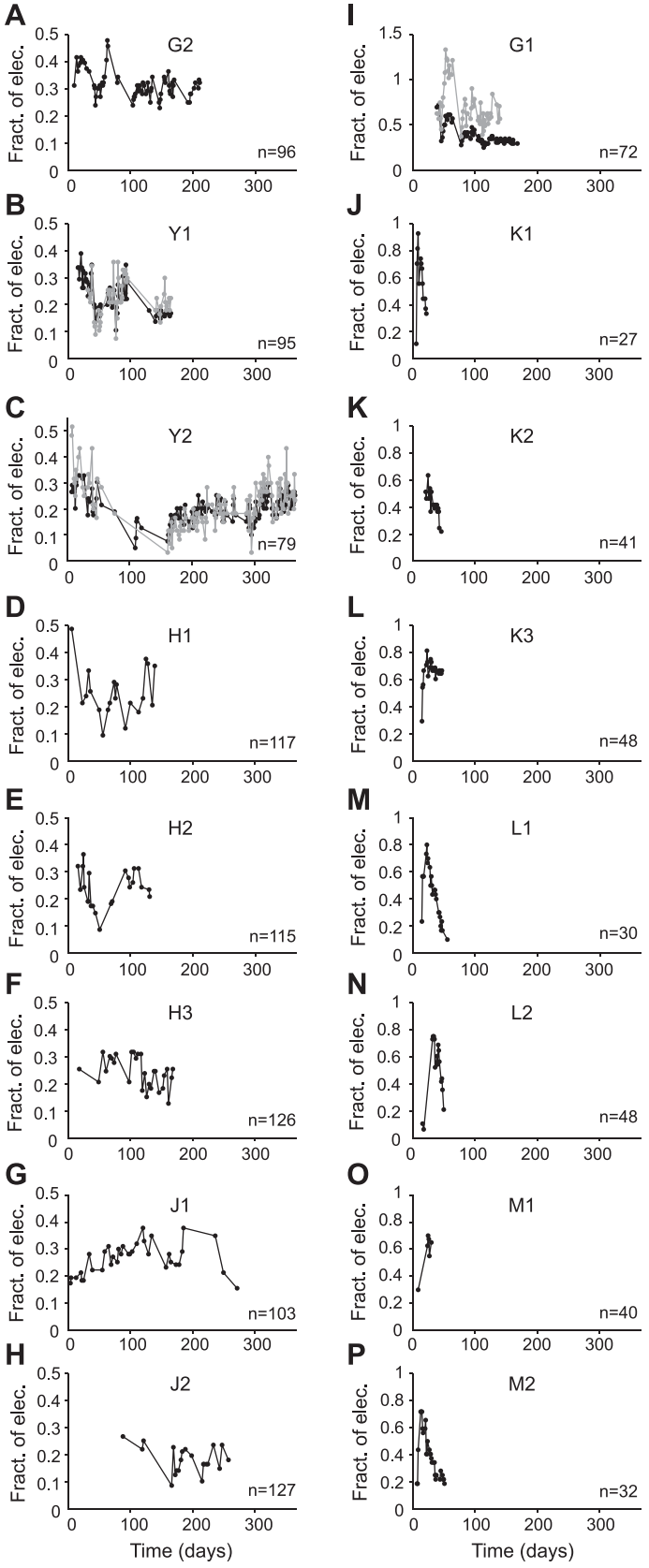

Fig. 6. Yield of individual implants across recording sessions. All electrodes were implanted in the brain on *day 0*. The number of electrodes in each implant (*n*) is noted in each panel. Vertical scales in the left column (*A–H*) are approximately half of those in the right column (*I–P*), to better illustrate differences in yield over time for those implants that had a lower maximum yield. The implants with shorter durations and smaller numbers of electrodes had higher maximum yields. Black lines: fraction of electrodes with recorded unit activity out of the total number of electrodes in each of 16 implants. Gray lines: number of isolated single units divided by the number of implanted electrodes targeting the FEF and CN (*B*, *C*, and *I*).

tion procedure (Suner et al. 2005), suggested that all of the units could be classified as "good" or "fair", as opposed to "poor" (Fig. 5*B*). For the same three sessions, we also analyzed the stability of recorded unit activity by computing the similarity of waveforms (Jackson and Fetz 2007) in the first and second halves of the session. Over 99% of the units were stable across time within individual recording sessions (Fig. 5*C*, $r \geq 0.98$).

To investigate the time course of the yield in individual implants, in each recording session of two monkeys (H and J, 5 implants total), we classified the electrodes that recorded unit activity into two groups: electrodes that had recorded units in the preceding session and electrodes that had not (Fig. 7). These two groups both contributed persistently to the yield over the course of each implant. Of the electrodes that recorded at least one unit in a given session, 35 ± 18% (mean ± SD unless otherwise noted) recorded new unit activity; that is, they had not recorded any units in the previous session (means for each implant in monkey H: 43 ± 16%, 35 ± 21%, and 44 ± 12%; in monkey J: 25 ± 13% and 32 ± 20%).

The emergence of new activity on many electrodes represents a key advantage of the ChIME system over immovable multielectrode arrays. New unit activity can, in principle, emerge spontaneously in experiments using immovable multielectrode arrays, but the percentage of new units appearing in immovable-array implants is likely low, as the electrodes cannot be moved to new sites. In implants using the ChIME system, by contrast, a substantial proportion of the recorded activity was due to new unit activity, which continued to arise for several months. The most likely reason for this is that the electrodes were moved, as others have shown using short-term implants of small numbers of movable electrodes (Cham et al. 2005; Muthuswamy et al. 2011). We therefore assessed the effect of manipulating the depths of the implanted electrodes on the yield. Because all electrodes were moved at least once during the course of a given implant, we focused on electrodes that were moved immediately before a given recording session.

Here we present an analysis of data from monkey H, because session yields did not differ significantly across all three implants in this monkey (χ^2 test, $P > 0.5$). Of the electrodes that recorded new unit activity in a given session, n, on average 37 ± 32% had been moved since the preceding session, $n - 1$ (Fig. 7, *A–C*). As this percentage varied with the rate at which electrodes were moved, it does not imply a causal relationship between moving electrodes and recording new unit activity. Focusing on the electrodes that had not recorded units in session $n - 1$, we asked whether moving them increased the likelihood of recording new units in the following session, n. In each of the three implants, we found that it did. Electrodes that had been moved were significantly more likely to record new units in the following session than electrodes that had not been moved (χ^2 test, $P < 10^{-15}$). This comparison does not take into

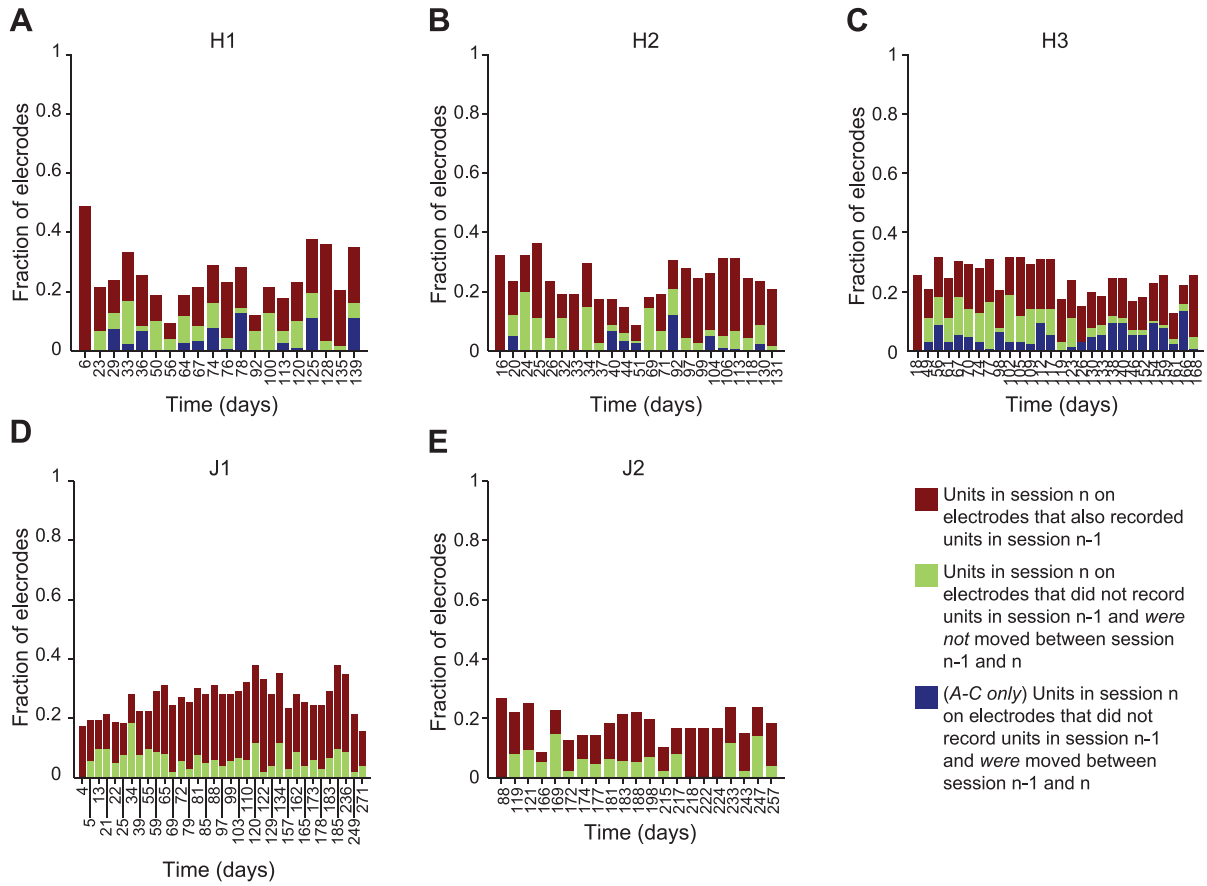

Fig. 7. Yield dynamics across recording sessions. All electrodes were implanted in the brain on *day 0*. *A–C*: for each session of implants 1–3 of monkey H, the fraction of units recorded in session n are broken down into 3 categories according to the activity during preceding sessions ($n - 1$). Red: unit also recorded in session $n - 1$. Green: unit not recorded in session $n - 1$ and electrode was not moved before session n. Blue: unit not recorded in session $n - 1$ and electrode was moved before session n. *D* and *E*: same as *A–C*, except that the electrodes that did not record units on session $n - 1$ were not subdivided according to the movement of the electrodes.

account the movement of electrodes in sessions $n - 2$ and earlier, and therefore likely underestimates the effect of moving electrodes on the yield. We examined the probability of obtaining unit activity only in the recording session immediately following a session in which an electrode was moved, and we did not take into account the cumulative effects of moving electrodes multiple times before new units were recorded, which likely give rise to most, if not all, of the new units (Fig. 7, green bars).

Session-to-session stability of neural activity. We tested the ability of the ChIME system to record neural activity during

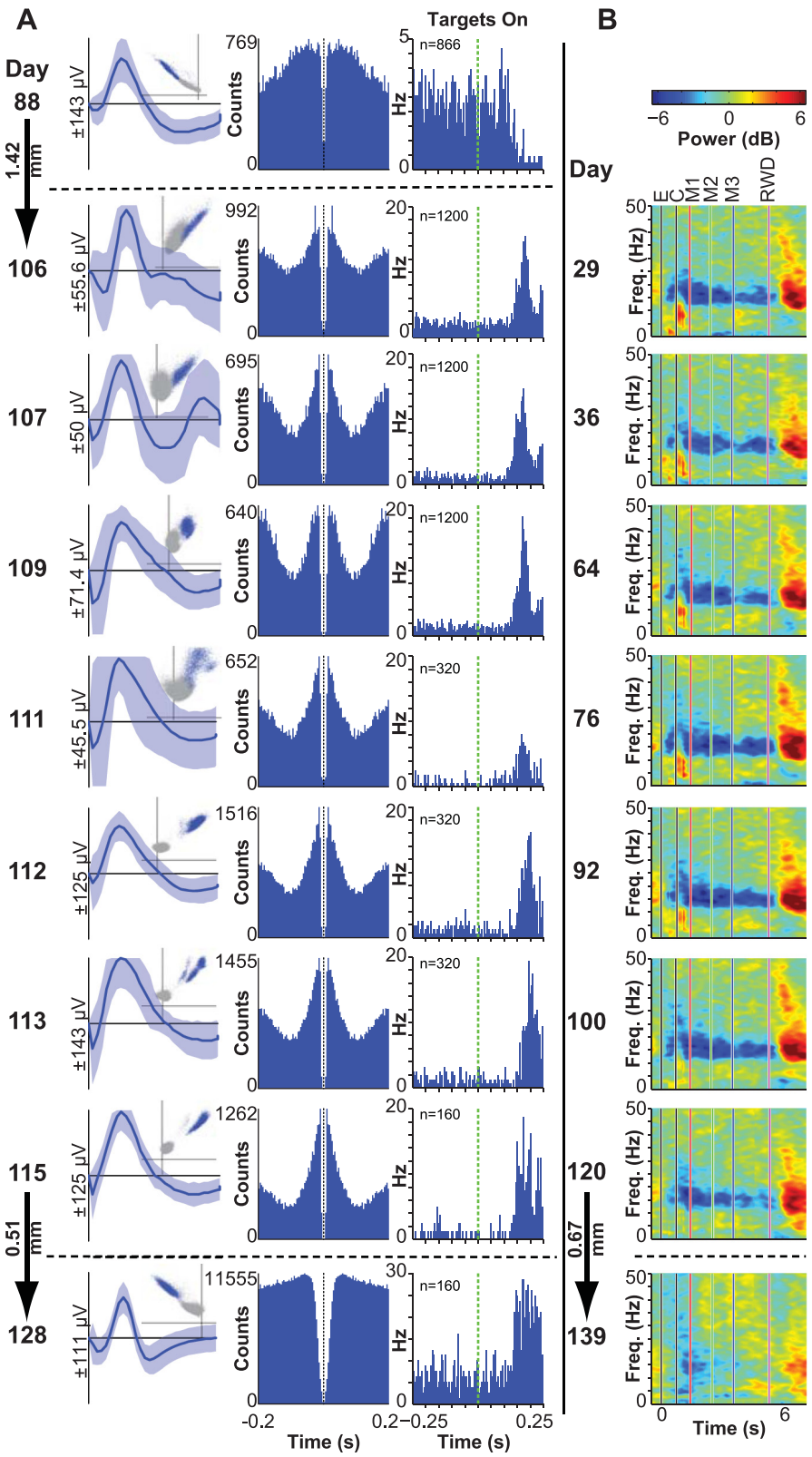

Fig. 8. Session-to-session stability of neural recordings. *A*: day of implant, mean wave shape (±3 SD) with inset of first principle component vs. peak-valley feature plot, autocorrelogram and perievent time histogram (PETH) aligned on the onset of visual targets (green line) for a single electrode targeting the CN in the chronic implant of monkey G during performance of the oculomotor scan task. Each row corresponds to a different recording session. Electrode was moved between *day 88* and *106* and again between *day 115* and *128*. The reduction in phasic unit firing in the PETH on *day 111* may be due to the introduction of a new visual task on that day. *B*: spectrograms from an electrode in the dlPFC of monkey H (implant 2) during performance of the joystick task. Aligning events are the same as in Fig. 3. Responses from the middle layers of area 9/46 are shown in recording sessions spanning 92 days. Electrode was moved to the deeper layers of 9/46 between *day 120* and *139*.

consecutive sessions from multiple electrodes that were not moved in the interim (Fig. 8). We analyzed the durations of such stretches of stable activity in six implants across three monkeys. On average, an electrode recorded unit activity in 2.1 ± 2.8 consecutive sessions (3.9 ± 8.5 days) without being moved. Stationary electrodes that recorded unit activity in at least two consecutive sessions recorded unit activity in a total of 4.2 ± 4.1 consecutive sessions (9.7 ± 12.8 days), on average. Not only did many electrodes retain unit activity across several days, but in some cases the activity recorded on a given electrode exhibited striking session-to-session similarities in wave shape, interspike interval distribution, and responses to behavioral task events (Fig. 8*A*, *days 106-115*), attributes typically used to identify stable units (Jackson and Fetz 2007; Suner et al. 2005). For the example shown in Fig. 8*A*, we computed the Pearson correlations between mean-subtracted, variance-normalized waveforms recorded in separate sessions, as a quantitative measure of the similarity of the clusters (Jackson and Fetz 2007). The correlations were 0.85, 0.96, and 0.98 between *days 106* and *109*, *109* and *112*, and *112* and *115*, respectively. The last of the three values is comparable to those reported for individual units within single sessions (Jackson and Fetz 2007, and our data presented above). LFPs recorded from stationary electrodes also showed extraordinary stability over periods of several weeks to months (Fig. 8*B*; see also Fujii and Graybiel 2005, Fig. 4). When the electrodes were moved, the recorded spike and LFP signals changed noticeably (Fig. 4, *B* and *C*; Fig. 8*A* first and last day; Fig. 8*B*, last day) and the correlation values measuring the similarity of the wave shapes decreased, as well (0.82 for *days 88* and *106*, when the electrode moved 1.42 mm; and 0.72 for *days 115* and *128*, when the electrode moved 0.51 mm). This demonstrates that small changes in electrode depth could result in detectable changes in neural activity and suggests that the recordings made before moving the electrode were obtained from relatively small volumes of brain with similar functional properties.

Microstimulation and injection using the ChIME system. We have exploited the versatility of the ChIME system to incorporate electrical stimulation and pharmacological injection methods with chronic recordings of neural activity. In a subset of experiments, we tested for within-area modulation of spike activity using single-pulse electrical stimuli in the ACC. We found fixed, short-latency responses from multiple simultaneously recorded units in the ACC, indicating synaptic connectivity between sites targeted by the chronically implanted electrodes (Fig. 9). The stimulation-evoked responses were sufficiently localized so that units recorded in the CMA did not respond to the ACC stimulation. Moreover, on electrodes that recorded multiple units in the ACC, not all single units exhibited a significant response (Fig. 9*A*) and stimulation artifact was easily discriminated from stimulation-evoked responses (Fig. 9, *B* and *C*). In separate experiments, we used electrical stimulation to detect functional connectivity between brain regions. By stimulating at four sites in the dlPFC, we found differential modulation of the LFP activity recorded simultaneously at multiple sites in the CN (Fig. 10*A*).

We have also begun to develop injection methods for use with the ChIME system. In pilot experiments, we recorded units in dlPFC and CN simultaneously and examined their responses to injections made in the CN. In the example shown in Fig. 10*B*, all four of the striatal units exhibited changes in firing rate, whereas none of the eight prefrontal units showed changes in firing rate for up to 10 min following the injection. This example demonstrates the possibility of using the ChIME system to perform pharmacological manipulations of subsets of recording sites in the context of an extended-duration implant. Stimulation and injection techniques can be used to search for and identify desired recording sites, as well as to record the neural and behavioral effects of localized electrical or pharmacological manipulations, making the ChIME system a powerful tool for studying the functions of brain circuits.

DISCUSSION

Large-scale simultaneous recordings from multiple superficial and deep brain structures test the limits of existing methods for extracellular recordings in alert nonhuman primates. We developed the ChIME system to meet this need. It is the first system to enable simultaneous recordings from tens and potentially hundreds of individually movable electrodes implanted chronically across several superficial and deep structures in the nonhuman primate brain. The most important advantage of the ChIME system is the opportunity it provides to sample neural activity at multiple depths chronically and flexibly. The ability to move individual electrodes can dramatically improve the yield of single units, as demonstrated by the comparison of the unit activity between electrodes that had or had not been moved across pairs of successive sessions. The single-unit yields in the initial recording sessions of each implant were similar to those reported for experiments using immovable electrode arrays, chronically implanted in multiple cortical areas (Chhatbar et al. 2010; Nicolelis et al. 2003). However, the ability to move electrodes at will over the lifetime of the implant led to sustained yields over the long term, in marked contrast to the time-dependent deterioration of yields typically seen with immovable electrode arrays (Liu et al. 2006; Muthuswamy et al. 2011).

Fig. 9. Cortico-cortical connectivity demonstrated by electrical stimulation in ACC. *A*: histograms of the spiking activity of single units recorded simultaneously from 8 chronically implanted electrodes in the cingulate cortex during 500 stimulation trials aligned on stimulation onset (bin width, 0.1 ms). Electrical stimuli were delivered between 2 chronically implanted electrodes in the ACC (bipolar microstimulation: anode and cathode indicated by + and -, pulse width: 0.2 ms, current amplitude: 70 μA). Of the 15 units simultaneously recorded in the ACC and cingulate motor area (CMA), 7 units showed significant responses to the stimulation (beyond the 99% confidence limits estimated from the prestimulation baseline firing rates) within 10 ms of the stimulus. *B*: unfiltered, inverted field potential recorded from ACC electrode 2 (shown in *A*), aligned on stimulation onset (*time zero*). The first 20 stimulation trials are shown (from top to bottom). An evoked field potential (framed by red rectangle) was consistently observed ~2.5 ms following the stimulation. The timing of the evoked potential was substantially more variable across trials than the stimulation artifacts were. The short-latency evoked potential shown was not observed on the other simultaneously recorded electrodes. Following the evoked potential, a significant increase in the spiking activity (shaded red rectangles) of 2 units was observed (from 1.8 Hz and 0.5 Hz prestimulation to >10 Hz poststimulation for both units). *C*: first (*x*-axis) and second (*y*-axis) principal components of the waveforms recorded with ACC electrode 2 formed 5 distinct clusters: 2 single units (yellow and blue), 2 evoked potential shapes (green and red), and the stimulation artifact (black). The overlaid waveforms of each cluster are also shown.

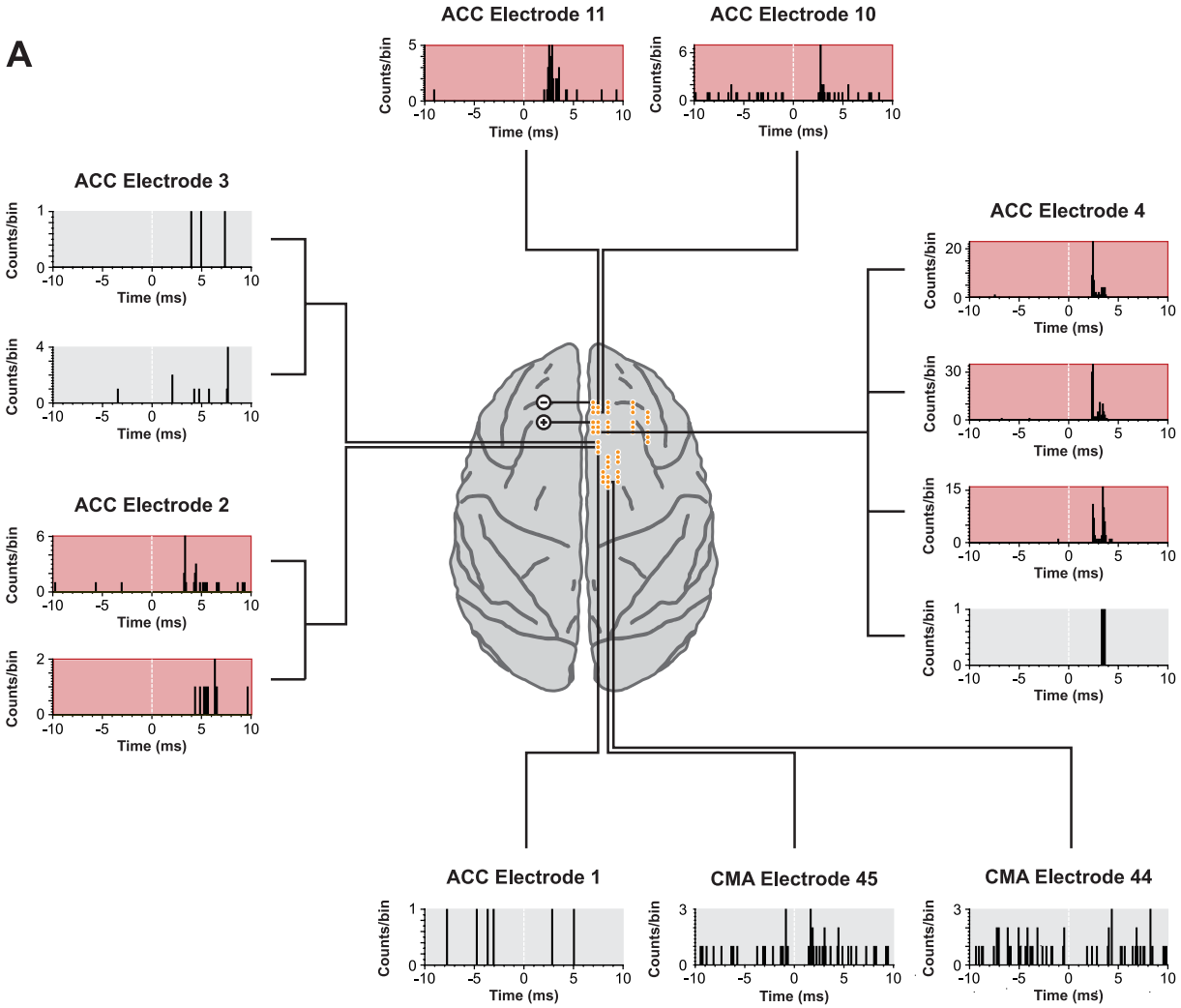

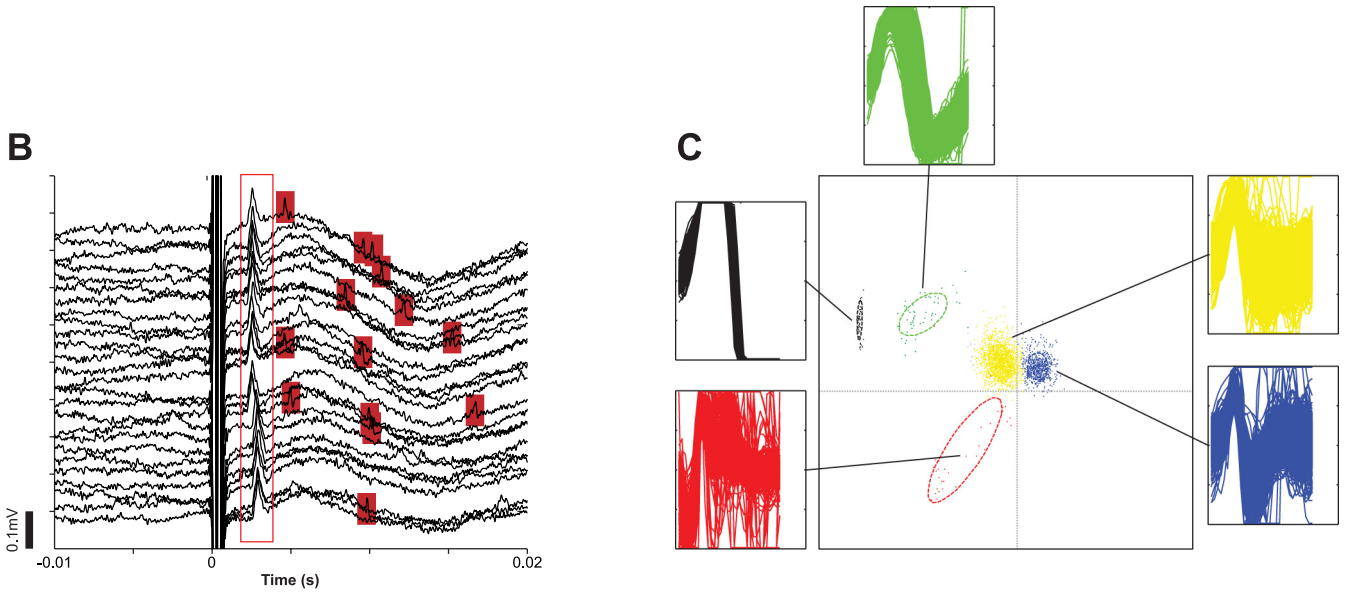

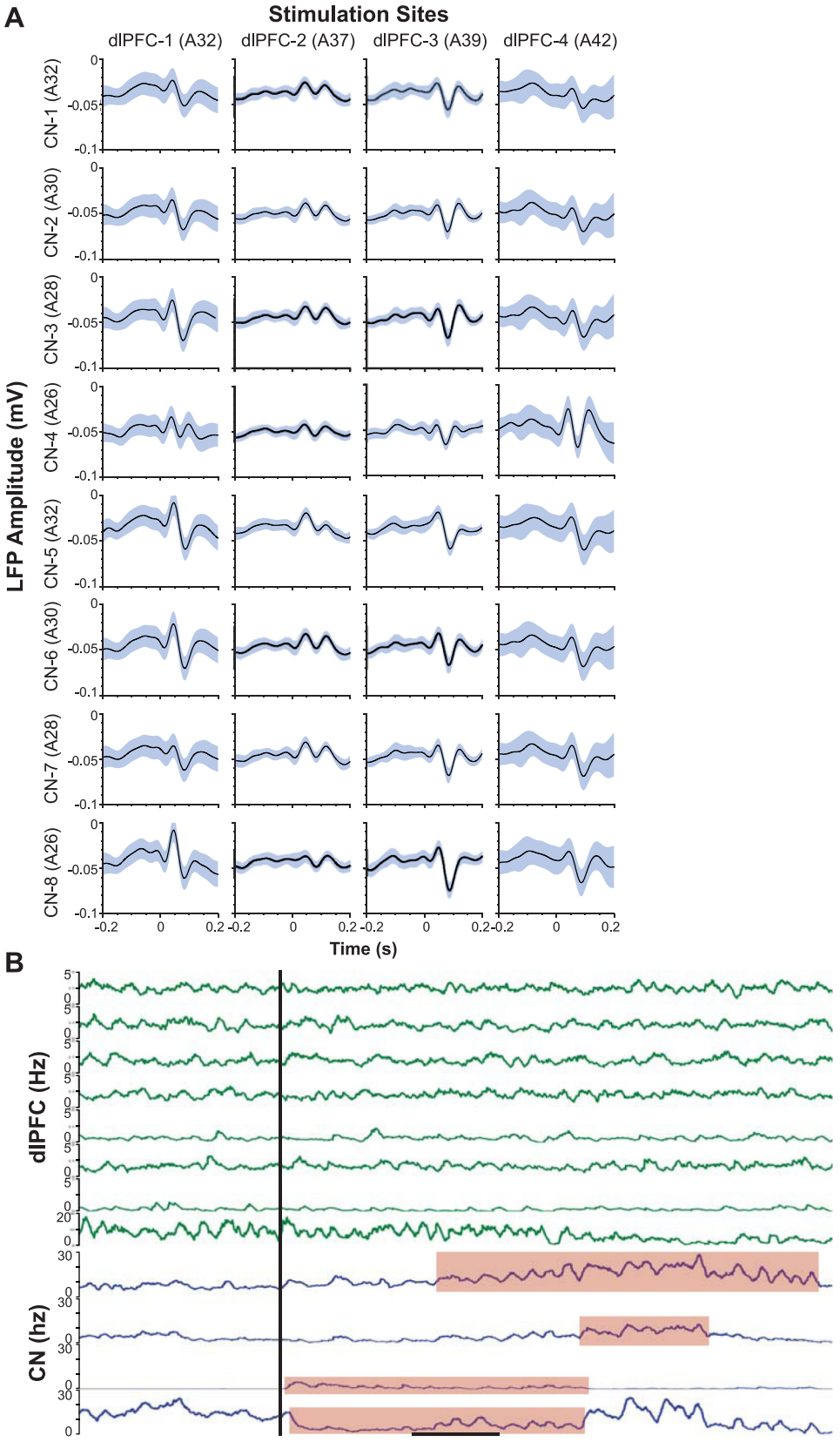

Fig. 10. *A*: selective modulation of LFPs in CN by electrical stimulation in dlPFC. For each of 4 stimulation locations in dlPFC, averages of LFP waveforms recorded simultaneously from 8 electrodes chronically implanted in the CN are shown, aligned on the onset of stimulation (40 trials; blue shading, 95% confidence intervals). Different striatal sites exhibited significant modulation, depending on the stimulation site in dlPFC. *B*: localized neural effects of a subcortical pharmacological injection. The firing rates of simultaneously recorded neurons in the dlPFC (*top*) and head of the CN (*bottom*) are shown aligned on the onset time of drug injection in the CN (vertical black line), using the ChIME system. The striatal, but not prefrontal, units exhibited significant changes in firing rate (pink shading) after drug infusion, compared with average predrug activity. Scale bar = 2 min.

In addition to its critical effect on the yield, the independent manipulation of electrodes enabled recordings from different combinations of depths across the recording tracks of a single implant (Fig. 4). This cannot be done using silicon probes with multiple contacts, the distances between which are fixed (Kipke et al. 2003). The ability to use the ChIME system to sample different combinations of recording sites day to day creates novel opportunities for recording neural activity across distributed corticosubcortical networks in the primate brain. This is a considerable advantage of the ChIME system over immovable arrays, which have not been used to study subcortical structures of the primate brain because of the potential for substantial damage to the overlying cortex and white matter. Such damage has been observed in the brains of cats (McCreery et al. 2006). Furthermore, whereas there is little control over the types of neurons recorded with immovable arrays, by adjusting the depths of electrodes independently with the ChIME system, neurons that are anatomically connected (as confirmed by microstimulation) or that belong to specific classes (based on physiological characteristics and responses) can be targeted and studied selectively. Taken together, the numerous advantages of the movable electrodes implanted with the ChIME system thus provide a unique opportunity to collect neural data for analyzing circuits spanning cortical and deep structures.

Existing recording methods share some, but not all, of the features of the ChIME system. Jackson and Fetz (2007), and separately Wilson and colleagues (Sun et al. 2006), used chronically implanted, independently movable electrodes in the nonhuman primate. However, these methods were designed for use only with a small number of electrodes and primarily in the freely moving monkey. A method by Merzenich and colleagues (deCharms et al. 1999) used 49 electrodes but to record from a single cortical area of nonhuman primates with brains considerably smaller than those of macaques. It is not clear whether or how any of these or similar methods (Galashan et al. 2011) could be used to record simultaneously from multiple structures in the macaque brain, as we have done using the ChIME system. Other chronic recording methods using movable microwires have been developed for nonprimate species, including rabbits (Swadlow et al. 2005) and rodents (Jog et al. 2002; Johnson and Welsh 2003; Yamamoto and Wilson 2008). Adapting these methods to record from multiple cortical and deep structures in the macaque brain would require reducing the physical footprint of the microdrives substantially, as well as overcoming the challenge of traversing sulci with microwires, as opposed to the sharp microelectrodes used with the ChIME system.

Others have recorded neuronal activity in the monkey brain simultaneously from multiple structures (Buschman and Miller 2007; Hernandez et al. 2008; Pasupathy and Miller 2005) or from multiple sites within a single structure (Baker et al. 1999; Courtemanche et al. 2003; Gray et al. 2007) using acute methods, in which the electrodes were implanted daily. Recordings commenced within a few hours following electrode implantation, and the electrodes were extracted from the brain at the end of each recording session. These acute multielectrode methods require considerable preparation time before each recording session, constraining the duration and frequency of experimental sessions. These methods have additional drawbacks, including the difficulty of maintaining stable signals following the acute implantation of multiple electrodes in a confined region, an increased potential for tissue damage from repeated daily penetrations of the dura mater and brain, and the inability to track learning-related changes in the activity of a localized neural population across daily recording sessions. Most importantly, the maximum number of independently movable drives that can be implanted acutely is likely to be at least one order of magnitude smaller than what can be achieved with the ChIME system.

In our experiments using the ChIME system, the neural signals on many electrodes were stable across numerous sessions (Figs. 7 and 8). The durations of periods of stable activity recorded by individual electrodes were likely limited by the fact that most of the electrodes in an implant were moved periodically to sample new sites along each track. Moving electrodes could have reduced the stability of signals recorded on neighboring stationary electrodes. We suspect that the long-term stability of signals recorded with the ChIME system is due to the combination of continued growth of granulation tissue overlying the exposed dura mater within the chamber and to the multiple guide tubes stabilizing the dural surface. It is possible for the dura mater and overlying calvarium to regrow over the course of several weeks, providing even further stabilization of the electrodes. Indeed, we found evidence for dural adhesions to the guide tubes in at least one monkey that was perfused with the implanted electrodes left in place (see MATERIALS AND METHODS).

As signal quality was often maintained day to day, minimal prerecording preparation time was required, with the bulk of it spent adjusting electrode depths to improve single-unit isolation. On any given day, we only adjusted the depths of a fraction of the electrodes. With implants of greater numbers of electrodes, we moved electrodes only on nonrecording days. This made the system essentially "plug-and-play" on recording days, maximizing the length of recording sessions.

The number of electrodes used in our experiments to date has been limited only by the capacity of available data-acquisition systems. We have demonstrated the capabilities of the ChIME system using commercially available, epoxy-coated tungsten or parylene-coated Pt/Ir microelectrodes, but we have successfully tested the use of microwire bundles to increase the density of recording sites by increasing the number of recording channels per track. These could be substituted by tetrodes, stereotrodes, or multicontact probes, all of which can be attached to a microdrive screw. The number of simultaneously recorded channels could also be increased by adding more microdrives, which can drive ~9 tracks per 30 grid holes, allowing up to ~450 tracks in a single implant (using a 40 mm × 40 mm grid).

The flexibility of the ChIME system permits the incorporation of other methods in conjunction with electrode-based recordings. Electrical stimulation can be used to map the functional connectivity within and across brain regions over the course of a chronic implant (Figs. 9 and 10*A*). Microinjections can be made through the grid to perform pharmacological manipulations and anatomical labeling (Fig. 10*B*). Fiber optics can be passed through the grid for use with optogenetic methods, which have recently been extended to the monkey brain (Diester et al. 2011; Han et al. 2009). With minor changes (e.g., replacing the microdrive screws with plastic ones), the ChIME system could also be used in paired record-

ing and functional MR-imaging experiments. Using these and other innovative techniques with the ChIME system should make it possible to manipulate and record chemical, electrical, and optical signals in nearby tracks simultaneously over long periods of time, giving unprecedented insight into the circuit-level functions of cortical and subcortical networks.

The gradual deterioration of signal quality is a challenge facing all chronic recording methods. The falloff in yield and accompanying increase in the impedance of many electrodes over the course of an implant has been attributed to the process of gliosis (Stice and Muthuswamy 2009). The ChIME system can be used to reduce the effects of gliosis by moving the electrodes. Nevertheless, in our experience, the SNR tended to degrade over the duration of the implant along with the proportion of well-isolated single units. Using Pl/Ir electrodes, we have been able to reduce electrode impedances by stimulating frequently to "clean" the electrode tips (Otto et al. 2006). The stimulation paradigm effectively reduced even high impedances (>2 MOhm) to preimplant levels. However, stimulation typically did not lead to new unit activity unless the electrodes were subsequently moved.

A potential drawback of the ChIME system, shared by other implant systems, is that the approach of some of the electrodes is not orthogonal to the cortical surface (Fig. 2*D*). This can present a challenge for targeting some cortical areas. When necessary, we have addressed this issue by implanting some chambers above a single hemisphere, targeting structures along up to 50 mm of the anterior-posterior axis. This orients most of the grid in parallel to the underlying cortical surface. We have also used smaller chambers (e.g., 30 mm × 30 mm), placed at an angle and offset from the midline.

The ChIME system successfully resolves two major problems associated with current recording techniques: a low rate of data acquisition and the inability to measure the activity of many neurons simultaneously across superficial and deep brain structures. The main advantages of our system include the ability to sample from a variety of cortical and subcortical locations simultaneously, the possibility of changing the recording locations over days, the increased yield resulting from moving electrodes, the ability to sample activity from small volumes of brain with excellent stability over weeks, minimal daily preparation and maintenance, the ability to reimplant monkeys in the same or different brain regions, and the possibility of interfacing with a variety of electrodes and experimental techniques. These key features combine to make a powerful, simple to use, chronic recording system that we anticipate will contribute to an understanding of the function of multiple interacting circuits widely distributed across the brain.

ACKNOWLEDGMENTS

We thank P. Blazquez, H. F. Hall, M. Cantor, N. Hasegawa, B. DePasquale, A. Quach, P. Harlan, R. Marini, C. Keller-McGandy, M. Histed, Y. Kubota, B. Baker, G. Fakterman, E. Romano, A. McWhinnie, and M. C. Brown for help.

GRANTS

This work was supported by the National Institutes of Health Javits Merit Grant NS025529, National Eye Institute Grant EY012848, Office of Naval Research Grant N000140710903, DARPA Grant NBCHC070105, and the Stanley H. and Sheila G. Sydney Fund (A. Graybiel), MIT Zakhartchenko Fellowship (J. Feingold), and NDSEG Fellowship (T. Desrochers).

DISCLOSURES

R. Harlan manufactures and sells components of the implant system but did not participate in performing experiments, analyzing data, interpreting results, or drafting, editing, and revising manuscript, except for a figure describing the implant system.

AUTHOR CONTRIBUTIONS

Author contributions: J.F., T.M.D., N.F., R.H., P.L.T., K.A., and A.M.G. conception and design of research; J.F., T.M.D., N.F., P.L.T., H.S., and K.A. performed experiments; J.F., T.M.D., N.F., P.L.T., and K.A. analyzed data; J.F., T.M.D., N.F., P.L.T., K.A., and A.M.G. interpreted results of experiments; J.F., T.M.D., R.H., P.L.T., and K.A. prepared figures; J.F. and T.M.D. drafted manuscript; J.F., T.M.D., N.F., P.L.T., K.A., and A.M.G. edited and revised manuscript; A.M.G. approved final version of manuscript.

REFERENCES

Alexander GE, DeLong MR, Strick PL. Parallel organization of functionally segregated circuits linking basal ganglia and cortex. *Annu Rev Neurosci* 9: 357–381, 1986.

Baker SN, Philbin N, Spinks R, Pinches EM, Wolpert DM, MacManus DG, Pauluis Q, Lemon RN. Multiple single unit recording in the cortex of monkeys using independently moveable microelectrodes. *J Neurosci Methods* 94: 5–17, 1999.

Buschman TJ, Miller EK. Top-down versus bottom-up control of attention in the prefrontal and posterior parietal cortices. *Science* 315: 1860–1862, 2007.

Carmena JM, Lebedev MA, Crist RE, O'Doherty JE, Santucci DM, Dimitrov DF, Patil PG, Henriquez CS, Nicolelis MA. Learning to control a brain-machine interface for reaching and grasping by primates. *PLoS Biol* 1: E42, 2003.

Cham JG, Branchaud EA, Nenadic Z, Greger B, Andersen RA, Burdick JW. Semi-chronic motorized microdrive and control algorithm for autonomously isolating and maintaining optimal extracellular action potentials. *J Neurophysiol* 93: 570–579, 2005.

Chhatbar PY, von Kraus LM, Semework M, Francis JT. A bio-friendly and economical technique for chronic implantation of multiple microelectrode arrays. *J Neurosci Methods* 188: 187–194, 2010.

Cohen MR, Maunsell JH. Attention improves performance primarily by reducing interneuronal correlations. *Nat Neurosci* 12: 1594–1600, 2009.

Contreras D, Destexhe A, Sejnowski TJ, Steriade M. Control of spatiotemporal coherence of a thalamic oscillation by corticothalamic feedback. *Science* 274: 771–774, 1996.

Courtemanche R, Fujii N, Graybiel AM. Synchronous, focally modulated beta-band oscillations characterize local field potential activity in the striatum of awake behaving monkeys. *J Neurosci* 23: 11741–11752, 2003.

Crist CF, Yamasaki DS, Komatsu H, Wurtz RH. A grid system and a microsyringe for single cell recording. *J Neurosci Methods* 26: 117–122, 1988.

deCharms RC, Blake DT, Merzenich MM. A multielectrode implant device for the cerebral cortex. *J Neurosci Methods* 93: 27–35, 1999.

Diester I, Kaufman MT, Mogri M, Pashaie R, Goo W, Yizhar O, Ramakrishnan C, Deisseroth K, Shenoy KV. An optogenetic toolbox designed for primates. *Nat Neurosci* 14: 387–397, 2011.

Ecker AS, Berens P, Keliris GA, Bethge M, Logothetis NK, Tolias AS. Decorrelated neuronal firing in cortical microcircuits. *Science* 327: 584–587, 2010.

Evarts EV. Relation of pyramidal tract activity to force exerted during voluntary movement. *J Neurophysiol* 31: 14–27, 1968.

Fujii N, Graybiel AM. Time-varying covariance of neural activities recorded in striatum and frontal cortex as monkeys perform sequential-saccade tasks. *Proc Natl Acad Sci USA* 102: 9032–9037, 2005.

Fujii N, Hihara S, Iriki A. Dynamic social adaptation of motion-related neurons in primate parietal cortex. *PLos One* 2: e397, 2007.

Funahashi S, Bruce CJ, Goldman-Rakic PS. Mnemonic coding of visual space in the monkey's dorsolateral prefrontal cortex. *J Neurophysiol* 61: 331–349, 1989.

Galashan FO, Rempel HC, Meyer A, Gruber-Dujardin E, Kreiter AK, Wegener D. A new type of recording chamber with an easy-to-exchange microdrive array for chronic recordings in macaque monkeys. *J Neurophysiol* 105: 3092–3105, 2011.

Gray CM, Goodell B, Lear A. Multichannel micromanipulator and chamber system for recording multineuronal activity in alert, non-human primates. *J Neurophysiol* 98: 527–536, 2007.

Graybiel AM, Rauch SL. Toward a neurobiology of obsessive-compulsive disorder. *Neuron* 28: 343–347, 2000.

Hammond C, Bergman H, Brown P. Pathological synchronization in Parkinson's disease: networks, models and treatments. *Trends Neurosci* 30: 357–364, 2007.

Han X, Qian X, Bernstein JG, Zhou HH, Franzesi GT, Stern P, Bronson RT, Graybiel AM, Desimone R, Boyden ES. Millisecond-timescale optical control of neural dynamics in the nonhuman primate brain. *Neuron* 62: 191–198, 2009.

Hernandez A, Nacher V, Luna R, Alvarez M, Zainos A, Cordero S, Camarillo L, Vazquez Y, Lemus L, Romo R. Procedure for recording the simultaneous activity of single neurons distributed across cortical areas during sensory discrimination. *Proc Natl Acad Sci USA* 105: 16785–16790, 2008.

Hochberg LR, Serruya MD, Friehs GM, Mukand JA, Saleh M, Caplan AH, Branner A, Chen D, Penn RD, Donoghue JP. Neuronal ensemble control of prosthetic devices by a human with tetraplegia. *Nature* 442: 164–171, 2006.

Jackson A, Fetz EE. Compact movable microwire array for long-term chronic unit recording in cerebral cortex of primates. *J Neurophysiol* 98: 3109–3118, 2007.

Jog MS, Connolly CI, Kubota Y, Iyengar DR, Garrido L, Harlan R, Graybiel AM. Tetrode technology: advances in implantable hardware, neuroimaging, and data analysis techniques. *J Neurosci Methods* 117: 141–152, 2002.

Johnson JL, Welsh JP. Independently movable multielectrode array to record multiple fast-spiking neurons in the cerebral cortex during cognition. *Methods* 30: 64–78, 2003.

Kipke DR, Vetter RJ, Williams JC, Hetke JF. Silicon-substrate intracortical microelectrode arrays for long-term recording of neuronal spike activity in cerebral cortex. *IEEE Trans Neural Syst Rehabil Eng* 11: 151–155, 2003.

Lei Y, Sun N, Wilson FA, Wang X, Chen N, Yang J, Peng Y, Wang J, Tian S, Wang M, Miao Y, Zhu W, Qi H, Ma Y. Telemetric recordings of single neuron activity and visual scenes in monkeys walking in an open field. *J Neurosci Methods* 135: 35–41, 2004.

Liu X, McCreery DB, Bullara LA, Agnew WF. Evaluation of the stability of intracortical microelectrode arrays. *IEEE Trans Neural Syst Rehabil Eng* 14: 91–100, 2006.

Luppino G, Matelli M, Camarda RM, Gallese V, Rizzolatti G. Multiple representations of body movements in mesial area 6 and the adjacent cingulate cortex: an intracortical microstimulation study in the macaque monkey. *J Comp Neurol* 311: 463–482, 1991.

Matsuzaka Y, Aizawa H, Tanji J. A motor area rostral to the supplementary motor area (presupplementary motor area) in the monkey: neuronal activity during a learned motor task. *J Neurophysiol* 68: 653–662, 1992.

McCreery D, Lossinsky A, Pikov V, Liu X. Microelectrode array for chronic deep-brain microstimulation and recording. *IEEE Trans Biomed Eng* 53: 726–737, 2006.

Mitz AR, Wise SP. The somatotopic organization of the supplementary motor area: intracortical microstimulation mapping. *J Neurosci* 7: 1010–1021, 1987.

Muthuswamy J, Anand S, Sridharan A. Adaptive movable neural interfaces for monitoring single neurons in the brain. *Front Neurosci* 5: 94, 2011.

Nichols AM, Ruffner TW, Sommer MA, Wurtz RH. A screw microdrive for adjustable chronic unit recording in monkeys. *J Neurosci Methods* 81: 185–188, 1998.

Nicolelis MA, Dimitrov D, Carmena JM, Crist R, Lehew G, Kralik JD, Wise SP. Chronic, multisite, multielectrode recordings in macaque monkeys. *Proc Natl Acad Sci USA* 100: 11041–11046, 2003.

Nordhausen CT, Maynard EM, Normann RA. Single unit recording capabilities of a 100 microelectrode array. *Brain Res* 726: 129–140, 1996.

Otto KJ, Johnson MD, Kipke DR. Voltage pulses change neural interface properties and improve unit recordings with chronically implanted microelectrodes. *IEEE Trans Biomed Eng* 53: 333–340, 2006.

Pasupathy A, Miller EK. Different time courses of learning-related activity in the prefrontal cortex and striatum. *Nature* 433: 873–876, 2005.

Pennartz CM, Berke JD, Graybiel AM, Ito R, Lansink CS, van der Meer M, Redish AD, Smith KS, Voorn P. Corticostriatal Interactions during Learning, Memory Processing, and Decision Making. *J Neurosci* 29: 12831–12838, 2009.

Pesaran B, Nelson MJ, Andersen RA. Free choice activates a decision circuit between frontal and parietal cortex. *Nature* 453: 406–409, 2008.

Rivlin-Etzion M, Marmor O, Heimer G, Raz A, Nini A, Bergman H. Basal ganglia oscillations and pathophysiology of movement disorders. *Curr Opin Neurobiol* 16: 629–637, 2006.

Santra S, Das B. Subdural pressure and brain condition during propofol vs isoflurane—nitrous oxide anaesthesia in patients undergoing elective supratentorial tumour surgery. *Indian J Anaesth* 53: 44–51, 2009.

Siapas AG, Lubenov EV, Wilson MA. Prefrontal phase locking to hippocampal theta oscillations. *Neuron* 46: 141–151, 2005.

Sommer MA, Wurtz RH. Brain circuits for the internal monitoring of movements. *Annu Rev Neurosci* 31: 317–338, 2008.

Sommer MA, Wurtz RH. Composition and topographic organization of signals sent from the frontal eye field to the superior colliculus. *J Neurophysiol* 83: 1979–2001, 2000.

Stice P, Muthuswamy J. Assessment of gliosis around moveable implants in the brain. *J Neural Eng* 6: 046004, 2009.

Strick PL, Preston JB. Two representations of the hand in area 4 of a primate. I. Motor output organization. *J Neurophysiol* 48: 139–149, 1982.

Sun NL, Lei YL, Kim BH, Ryou JW, Ma YY, Wilson FA. Neurophysiological recordings in freely moving monkeys. *Methods* 38: 202–209, 2006.

Suner S, Fellows MR, Vargas-Irwin C, Nakata GK, Donoghue JP. Reliability of signals from a chronically implanted, silicon-based electrode array in non-human primate primary motor cortex. *IEEE Trans Neural Syst Rehabil Eng* 13: 524–541, 2005.

Swadlow HA, Bereshpolova Y, Bezdudnaya T, Cano M, Stoelzel CR. A multi-channel, implantable microdrive system for use with sharp, ultra-fine "Reitboeck" microelectrodes. *J Neurophysiol* 93: 2959–2965, 2005.

Velliste M, Perel S, Spalding MC, Whitford AS, Schwartz AB. Cortical control of a prosthetic arm for self-feeding. *Nature* 453: 1098–1101, 2008.

Vetter RJ, Williams JC, Hetke JF, Nunamaker EA, Kipke DR. Chronic neural recording using silicon-substrate microelectrode arrays implanted in cerebral cortex. *IEEE Trans Biomed Eng* 51: 896–904, 2004.

Ward MP, Rajdev P, Ellison C, Irazoqui PP. Toward a comparison of microelectrodes for acute and chronic recordings. *Brain Res* 1282: 183–200, 2009.

Yamamoto J, Wilson MA. Large-scale chronically implantable precision motorized microdrive array for freely behaving animals. *J Neurophysiol* 100: 2430–2440, 2008.